

# Measurement Systems

---

## Final Project

Professor: Dr. Amini

Amirhossein Ansari 810600050

Hana Shamsaei 810600097

Summer 1404

Department of Mechanical Engineering

University of Tehran

# Abstract

The purpose of this project was to design and evaluate a simple measurement system capable of detecting the frequency of motion using electromagnetic induction and digital signal processing techniques. The setup consisted of a coil and a permanent magnet, where the movement of the magnet relative to the coil produced a time-varying voltage that was acquired by an Arduino board. The acquired data was then transferred to MATLAB for signal processing. A Fast Fourier Transform (FFT) algorithm was applied to the recorded voltage in order to identify the dominant frequency of the magnet's oscillatory motion.

Since the accuracy of frequency estimation depended heavily on the calibration of the coil-magnet system, different calibration strategies were investigated. Three approaches were designed and tested. In the first approach, a small DC motor with a cam mechanism was employed to generate periodic motion. Due to the limitations of the available power supply (5 V instead of 12 V), the motor could only reach a maximum frequency of approximately 1.7 Hz. In addition, the motor lacked sufficient torque to smoothly drive the cam and introduced magnetic noise into the measurements. As a result, this method was restricted to a single low-frequency calibration point and was not selected as a reliable option.

The second calibration method involved the use of a mechanical metronome. By setting the metronome to discrete frequencies ranging from 1 Hz to 5 Hz and manually moving the magnet in synchronization with the beat, the frequency response of the system was recorded. The FFT analysis showed very close agreement with the metronome frequencies, with only minor discrepancies due to spectral leakage. While this method provided confidence in the accuracy of the system within the low-frequency range, it was not suitable for extending calibration to higher frequencies, as manual oscillation beyond 5 Hz was impractical.

The final and most effective calibration method utilized the natural frequency of a cantilevered metal ruler. One end of the ruler was fixed to a table while a permanent magnet was attached to the free end. A coil was placed beneath the magnet, and the ruler was given an initial displacement to induce free vibrations. The induced voltage was recorded by the Arduino and analyzed using FFT. The experimental frequency results were compared with theoretical predictions obtained from beam vibration equations with an added tip mass representing the magnet. The agreement was strong, requiring only minor adjustments, and this method allowed calibration across a wider frequency spectrum than the previous approaches.

In conclusion, the study demonstrated that the coil-magnet system, when combined with FFT analysis, can reliably measure oscillation frequency. Among the three calibration methods tested, the cantilevered ruler method was identified as the most robust and practical, providing both accuracy and a broader usable frequency range. This approach highlights how simple experimental tools can be effectively combined with computational analysis to design low-cost frequency measurement systems for educational and research applications.

# Contents

<b>1</b>	<b>Introduction</b>	<b>4</b>
<b>2</b>	<b>Coil Design and Dimensioning</b>	<b>5</b>
2.1	Wire Diameter Verification . . . . .	5
2.2	Selection of Coil Diameter . . . . .	5
2.3	Choice of Number of Turns . . . . .	5
2.4	3D-Printed Coil Form and Final Winding . . . . .	5
<b>3</b>	<b>Ansys Maxwell Transient Simulation</b>	<b>7</b>
3.1	Model Setup . . . . .	7
3.2	Coil and Winding Definition . . . . .	7
3.3	Boundary Conditions . . . . .	8
3.4	Motion Setup . . . . .	9
3.5	Simulation Results . . . . .	9
3.6	Discussion and Validation . . . . .	10
3.7	Conclusion . . . . .	11
<b>4</b>	<b>Experimental Setup Design</b>	<b>12</b>
4.1	Main Setup . . . . .	12
4.2	Calibration Setup . . . . .	13
4.3	Comparison of Setups . . . . .	14
<b>5</b>	<b>Circuit Design</b>	<b>15</b>
5.1	Instrumentation Amplifier (AD620): $G = 20$ . . . . .	15
5.2	DC Offset (2.5 V) . . . . .	15
5.3	Noise Analysis and RC Filter . . . . .	16
<b>6</b>	<b>Calibration</b>	<b>17</b>
6.1	DC Motor Method . . . . .	17
6.1.1	Experimental Setup and Procedure . . . . .	18
6.1.2	Observations and Problems . . . . .	19
6.1.3	Conclusion on DC Motor Method . . . . .	20
6.2	Metronome Method . . . . .	22

6.3	Ruler Method . . . . .	26
6.4	Theory: Natural Frequency of the Cantilevered Ruler with a Tip Magnet (and Rotary Inertia) . . . . .	31
6.5	Curve Fitting and Calibration Curve . . . . .	34
<b>7</b>	<b>Appendix</b>	<b>38</b>
7.1	Arduino Code . . . . .	38
7.2	MATLAB code for getting data from Arduino . . . . .	40
7.3	MATLAB code for calculating ruler's natural frequency . . . . .	42
7.4	MATLAB code for plotting the calibration curve . . . . .	43

# 1 Introduction

Vibration measurement plays a critical role in engineering and applied sciences, particularly in areas such as structural health monitoring, machinery diagnostics, and control systems. Detecting vibrations accurately allows engineers to identify abnormal operating conditions, prevent failures, and ensure the safe operation of various mechanical and electronic systems. Conventional vibration sensors, such as accelerometers or piezoelectric devices, are widely used for these purposes. However, their relatively high cost and complexity often limit their accessibility for educational and experimental applications.

This project explores an alternative approach to vibration sensing through the application of **Faraday's Law of Electromagnetic Induction**. According to this law, a time-varying magnetic flux within a closed coil induces an electromotive force (EMF) proportional to the rate of change of the flux. In practical terms, when a magnet is set in oscillatory motion relative to a coil, a voltage signal is generated. This fundamental principle not only underlies many industrial sensors but also provides an excellent opportunity for building simple, low-cost devices capable of detecting vibration.

The main objective of this project is to **design, fabricate, and calibrate a homemade magnetic vibration sensor** that can detect vibration frequencies in the range of 1–10 Hz. The system consists of a permanent magnet mounted on a flexible cantilever element and a coil wound from enameled copper wire. As the magnet vibrates, the relative motion induces a measurable voltage in the coil. The signal is then captured and processed using an **Arduino microcontroller**, which extracts the dominant vibration frequency through digital techniques such as zero-crossing detection or Fast Fourier Transform (FFT).

Calibration is carried out using known vibration sources such as small DC motors with eccentric loads, ensuring that the measured frequency corresponds accurately to the actual input. In addition, the project emphasizes simplicity by relying on accessible materials and low-cost components, while still incorporating essential stages of design, experimentation, and validation. Optional simulation in Ansys Maxwell software further allows optimization of the sensor's geometry and electromagnetic performance.

Through this project, the underlying concepts of electromagnetic induction are directly applied in a hands-on engineering design, bridging theory with practice. The outcomes not only provide a functional sensor but also highlight the potential of low-cost, student-built devices in education and research.

## 2 Coil Design and Dimensioning

The geometry of the coil is a critical factor in determining the sensitivity and overall performance of the magnetic vibration sensor. In this project, the design process involved selecting the coil inner diameter, the wire diameter, and the total number of turns through a balance of electromagnetic performance, mechanical compatibility with the magnet, and practical considerations related to manual fabrication.

### 2.1 Wire Diameter Verification

The purchased wire was nominally specified as having a diameter of 0.50 mm. However, precise measurement using a digital caliper indicated an average diameter of 0.55 mm. Since coil dimensions, resistance, and packing density depend directly on the conductor size, the measured value was used for all subsequent calculations to ensure higher accuracy. The slightly thicker wire maintained sufficient mechanical robustness for hand winding while still allowing the desired number of turns within the available volume.

### 2.2 Selection of Coil Diameter

The inner diameter of the coil was set to 20 mm, chosen to provide optimal coupling with the 15 mm permanent magnet. A coil diameter slightly larger than the magnet ensures that the magnetic flux lines pass effectively through the coil cross-sectional area while leaving sufficient clearance for assembly. The induced electromotive force (EMF) depends on both the number of turns  $N$  and the effective coil area  $A = \pi(D/2)^2$ , as described by Faraday's law:

$$v(t) = -N \frac{d\Phi(t)}{dt} \approx -NA \frac{\partial B}{\partial x} \dot{x}(t),$$

where  $\dot{x}(t)$  is the relative velocity of the magnet and coil, and  $\partial B/\partial x$  is the magnetic field gradient. The value  $D = 20$  mm was therefore selected as a compromise: large enough to increase coil area  $A$ , yet small enough to maintain strong flux density from the magnet.

### 2.3 Choice of Number of Turns

The number of turns was fixed at  $N = 500$  to achieve adequate induced voltage levels while keeping the resistance at a manageable value. The total conductor length  $\ell$  can be estimated as

$$\ell = N_1 \pi [N_2(D + d) + d N_2(N_2 - 1)],$$

where  $N_1$  is the number of turns per layer,  $N_2 = \lceil N/N_1 \rceil$  is the number of layers,  $D$  is the inner coil diameter, and  $d$  is the measured wire diameter. For the chosen geometry ( $d = 0.55$  mm,  $D = 20$  mm,  $N = 500$ ,  $N_1 = 50$ ), the total wire length is approximately  $\ell = 40$  m. The corresponding DC resistance is

$$R \approx \rho_{\text{Cu}} \frac{\ell}{A_w}, \quad A_w = \pi \left( \frac{d}{2} \right)^2,$$

which gives  $R \approx 2.8 \Omega$  at room temperature. This resistance level is acceptable for minimizing noise and ensuring compatibility with the Arduino input circuit.

### 2.4 3D-Printed Coil Form and Final Winding

To facilitate precise and repeatable winding, a coil form (bobbin) was designed and fabricated using 3D printing. The bobbin was modeled with an inner cylindrical section corresponding to the desired coil diameter (20 mm), and flanges were added at both ends to maintain the alignment of the wire layers during the winding process. A small clearance of approximately 0.2 mm was introduced between the design diameter and the magnet dimension to ensure smooth assembly and removal.

The coil was then wound by hand using enameled copper wire of measured diameter 0.55 mm, achieving a total of 500 turns across multiple layers. The flanges of the printed bobbin prevented axial displacement of the wire and ensured a uniform build, as shown in Figure 1. The final dimensions closely matched the calculated design values, resulting in an outer coil diameter of approximately 31 mm and an axial length of 27.5 mm.

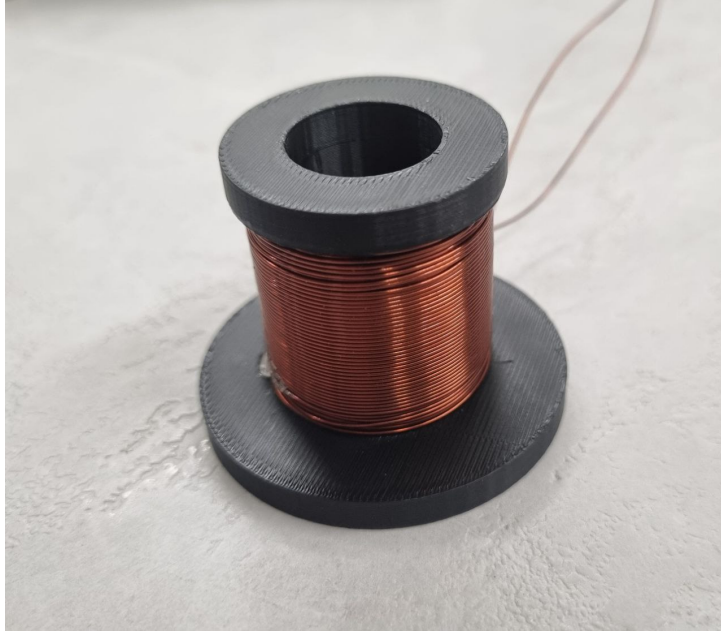


Figure 1: 3D-printed coil bobbin

### 3 Ansys Maxwell Transient Simulation

A 2D transient electromagnetic simulation was performed in **Ansys Maxwell 2024 R2** to evaluate the induced voltage of the designed coil under magnet vibration. The objective was to confirm the theoretical behavior predicted by Faraday’s law, verify that the selected coil geometry ( $N = 500$ ,  $D = 20$  mm, wire 0.55 mm) is appropriate, and estimate the output voltage level before physical testing.

#### 3.1 Model Setup

The simulation was created in **Maxwell 2D** with three material domains: copper (coil), NdFeB35 (permanent magnet), and vacuum (air region and motion band). Figure 2 shows the project tree, where each component is defined with its material and role in the simulation.

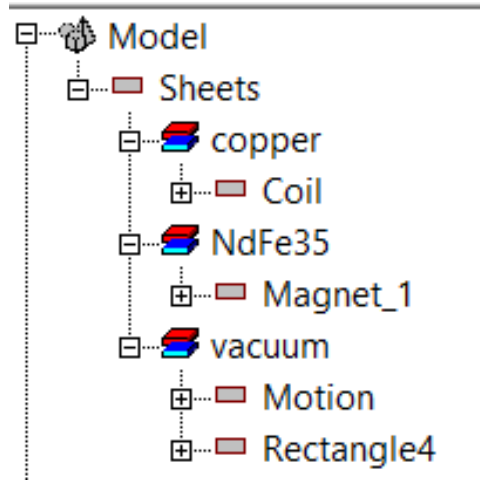


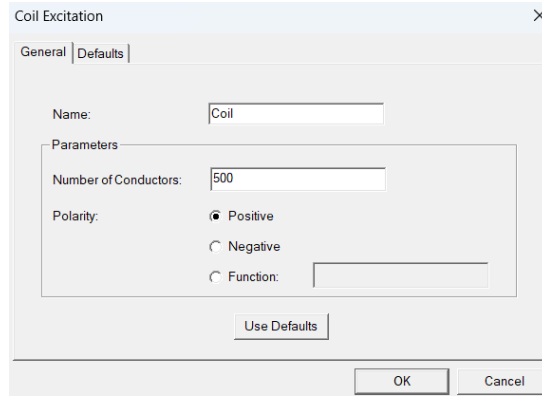
Figure 2: Model tree in Ansys Maxwell

The coil was modeled as a stranded winding with 500 turns, while the magnet was assigned NdFeB35 material with remanent flux density in the  $+Z$  direction. The surrounding vacuum box included a motion band for prescribing sinusoidal displacement of the magnet.

#### 3.2 Coil and Winding Definition

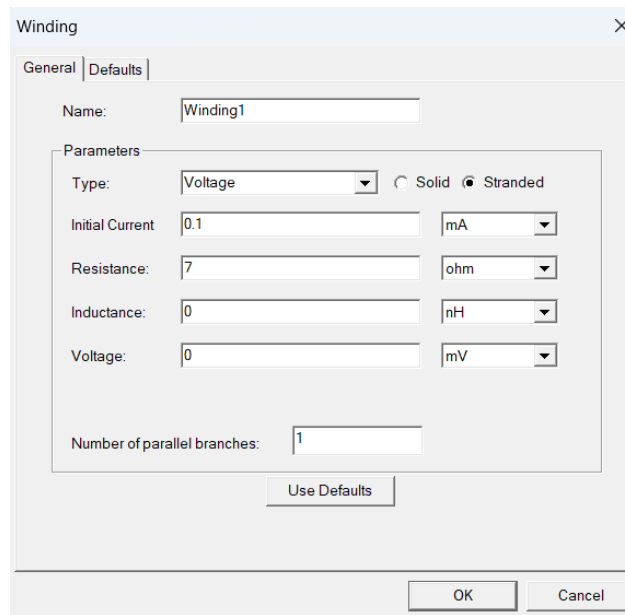
The coil excitation was set with 500 conductors and positive polarity (Fig. 3), corresponding to the experimentally built coil. A stranded winding setup was applied with a resistance of  $7\Omega$ , representing the measured DC resistance of the physical coil (Fig. 4).





The 'Coil Excitation' dialog box has a title bar with a close button (X). It contains two tabs: 'General' and 'Defaults'. The 'General' tab is active. It features a 'Name' field with the text 'Coil'. Below this is a 'Parameters' section containing a 'Number of Conductors' field with the value '500'. The 'Polarity' section has three radio buttons: 'Positive' (selected), 'Negative', and 'Function' (disabled). The 'Function' button is disabled because the 'Function' radio button is not selected. At the bottom of the 'Parameters' section is a 'Use Defaults' button. At the bottom of the dialog are 'OK' and 'Cancel' buttons.

Figure 3: Coil excitation setup



The 'Winding' dialog box has a title bar with a close button (X). It contains two tabs: 'General' and 'Defaults'. The 'General' tab is active. It features a 'Name' field with the text 'Winding1'. Below this is a 'Parameters' section. The 'Type' field is a dropdown menu set to 'Voltage'. To the right of the dropdown are two radio buttons: 'Solid' and 'Stranded' (selected). Below the 'Type' field are four rows of input fields: 'Initial Current' (0.1) with a unit dropdown (mA), 'Resistance' (7) with a unit dropdown (ohm), 'Inductance' (0) with a unit dropdown (nH), and 'Voltage' (0) with a unit dropdown (mV). At the bottom of the 'Parameters' section is a 'Number of parallel branches' field with the value '1'. At the bottom of the dialog are 'Use Defaults', 'OK', and 'Cancel' buttons.

Figure 4: Winding setup

### 3.3 Boundary Conditions

A vector potential boundary ( $A = 0$ ) was applied at the outer air box, as shown in Fig. 5, ensuring proper truncation of the computational domain and realistic free-space field conditions.

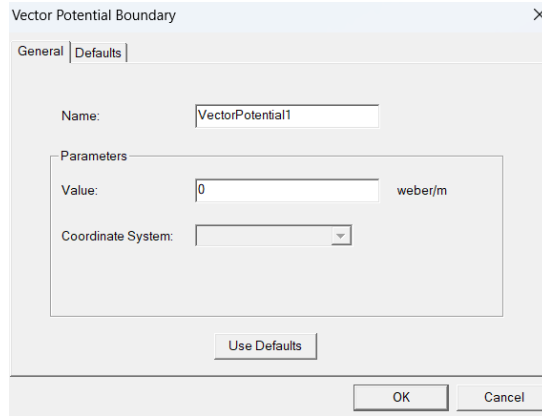


Figure 5: Vector potential boundary condition applied to the outer air region.

### 3.4 Motion Setup

The magnet was given a sinusoidal velocity profile to simulate vibration:

$$v(t) = 0.2 \cdot \sin(2\pi \cdot 5t) \quad [\text{m/s}],$$

corresponding to oscillation at 5 Hz with peak velocity 0.2 m/s. This produced a peak-to-peak displacement of approximately 10 mm. The motion setup window is shown in Fig. 6.

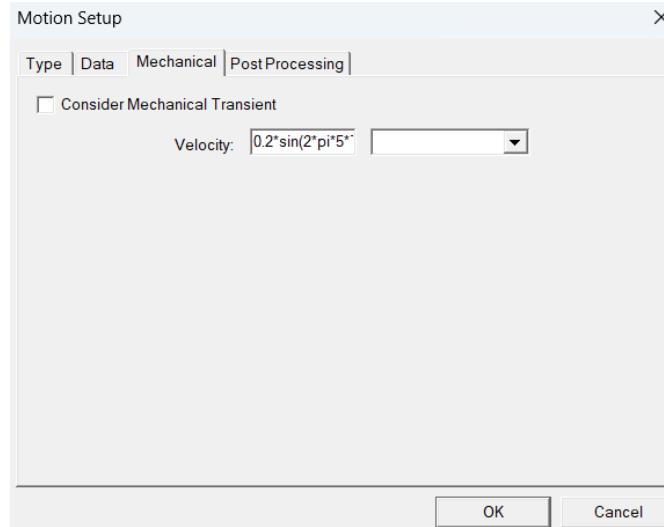


Figure 6: Motion setup for the permanent magnet with sinusoidal velocity input.

### 3.5 Simulation Results

The transient simulation ran for 1 s, covering five oscillation cycles. The results confirmed the expected behavior:

- **Position vs. time:** The magnet oscillated between 0 and 10 mm, as shown in Fig. 7.
- **Induced voltage vs. time:** The coil produced an alternating EMF waveform with polarity reversals at turning points, reaching amplitudes of approximately  $\pm 280$  mV (Fig. 8).

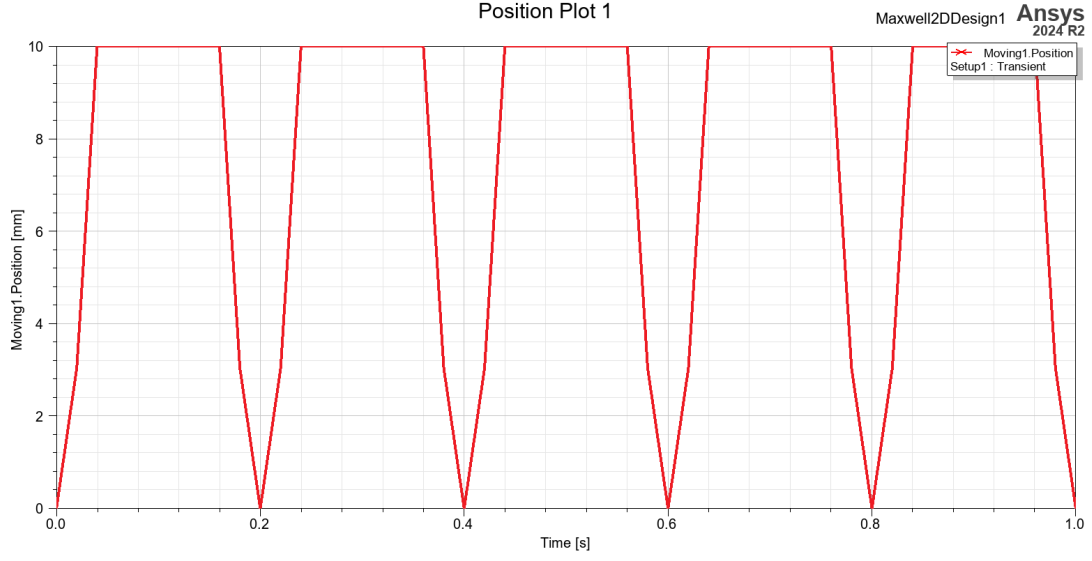


Figure 7: Magnet position vs. time, showing sinusoidal oscillation at 5 Hz.



Figure 8: Induced coil voltage waveform with peak amplitudes of about  $\pm 0.28$  V.

### 3.6 Discussion and Validation

The simulated waveform matched theoretical expectations based on Faraday's law:

$$v(t) = -N \frac{d\Phi}{dt} \approx -NA \frac{\partial B}{\partial x} \dot{x}(t).$$

The piecewise sinusoidal velocity generated alternating EMF proportional to coil area  $A$ , turn count  $N$ , and magnet speed  $\dot{x}(t)$ .

Importantly, the simulation confirmed that the chosen coil properties ( $N = 500$ ,  $D = 20$  mm,  $d = 0.55$  mm) were effective. The induced voltage amplitude of a few hundred millivolts falls within the range that can be safely amplified by the AD620 with  $G = 20$ , after adding the 2.5 V offset and low-pass filtering. This demonstrates that the design strikes a good balance between sensitivity and practicality.

### **3.7 Conclusion**

Using Ansys Maxwell, the selected coil and magnet configuration was validated prior to experimentation. The results showed that the designed coil dimensions and winding parameters produce a measurable EMF under realistic vibration conditions, confirming that the chosen coil properties are suitable for the sensor application.

## 4 Experimental Setup Design

Two different setups were designed and fabricated for the development and evaluation of the magnetic vibration sensor. The first one constitutes the main measurement setup, while the second was specifically constructed for calibration purposes. Both setups were designed using CAD software, 3D printed for structural parts, and assembled with standard components including the wound coil, magnet, and supporting beam.

### 4.1 Main Setup

The main setup, shown in Figures 9 and 10, consists of the 3D-printed coil positioned at the base, with a metallic cantilever beam fixed at one end and free at the other. A permanent magnet is mounted on the free end of the beam directly above the coil. Vibrations of the beam cause relative motion between the magnet and coil, thereby inducing a voltage according to Faraday's law. This configuration was used for the majority of measurements and experiments, as it provides a simple and direct method for detecting low-frequency vibrations in the range of 1–10 Hz.



Figure 9: Main experimental setup with coil, cantilever beam, and magnet.

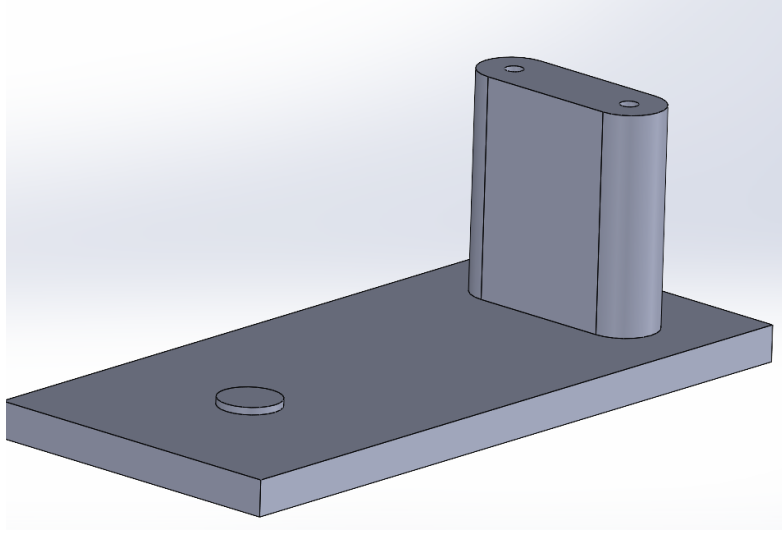


Figure 10: CAD model of the main setup.

## 4.2 Calibration Setup

For calibration, a second setup was designed to allow controlled excitation of the beam. As shown in Figures 11 and 12, this configuration includes a dedicated mounting location for a DC motor. A cam attached to the motor shaft converts the motor's rotational motion into periodic vertical displacement of the cantilever beam. By adjusting the motor speed, well-defined vibration frequencies can be generated. These reference vibrations were used to calibrate the sensor response, ensuring accurate frequency measurements from the Arduino processing system.

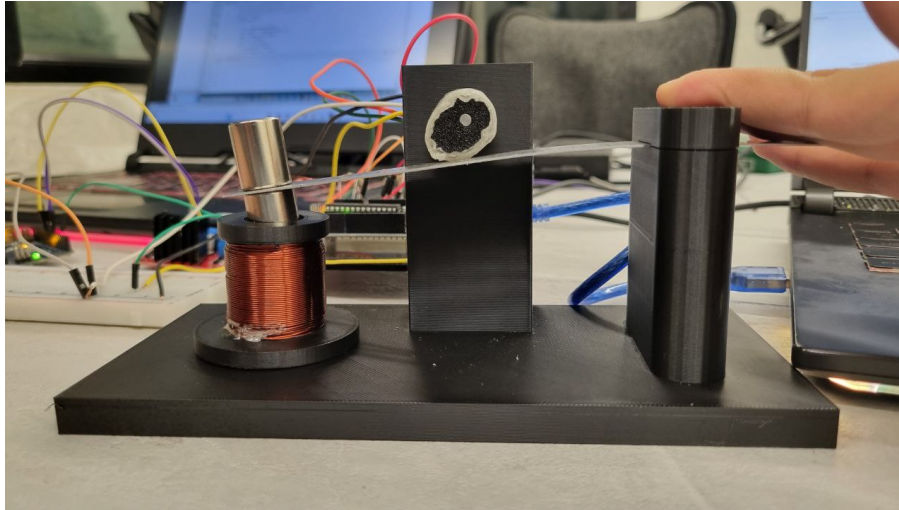


Figure 11: Calibration setup including space for DC motor and cam excitation mechanism.

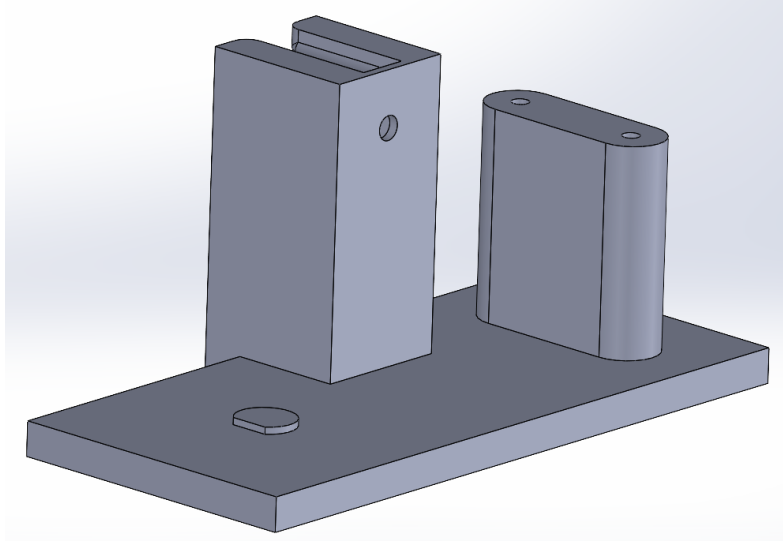


Figure 12: CAD model of the calibration setup with motor mounting position.

### 4.3 Comparison of Setups

The main setup provided a straightforward platform for experimental testing, focusing on natural vibration of the beam-magnet system. The calibration setup, on the other hand, offered precise control of excitation frequency using a motor-driven cam mechanism. Together, these setups enabled both qualitative testing and quantitative calibration of the magnetic vibration sensor.

## 5 Circuit Design

To condition the weak coil signal, the analog front end comprises an AD620 instrumentation amplifier, a 2.5 V DC offset stage, and a single-pole RC low-pass filter. This chain amplifies the millivolt-level EMF, shifts it into the Arduino's input range, and attenuates out-of-band noise.

### 5.1 Instrumentation Amplifier (AD620): $G = 20$

The AD620 was selected for its high input impedance and low noise. The target gain was fixed at

$$G = 20.$$

Using the AD620 relation

$$G = 1 + \frac{49.4 \text{ k}\Omega}{R_G},$$

the required gain-set resistor is

$$R_G = \frac{49.4 \text{ k}\Omega}{G - 1} = \frac{49.4 \text{ k}\Omega}{19} \approx 2.60 \text{ k}\Omega.$$

A standard 2.61 k $\Omega$  (E24) resistor or an equivalent parallel combination was used. The amplifier output feeds the offset and filtering stages.

### 5.2 DC Offset (2.5 V)

Because the Arduino ADC accepts only 0–5 V, the amplified bipolar signal is centered at 2.5 V via a precision divider/buffer, ensuring headroom for positive and negative excursions around mid-scale.

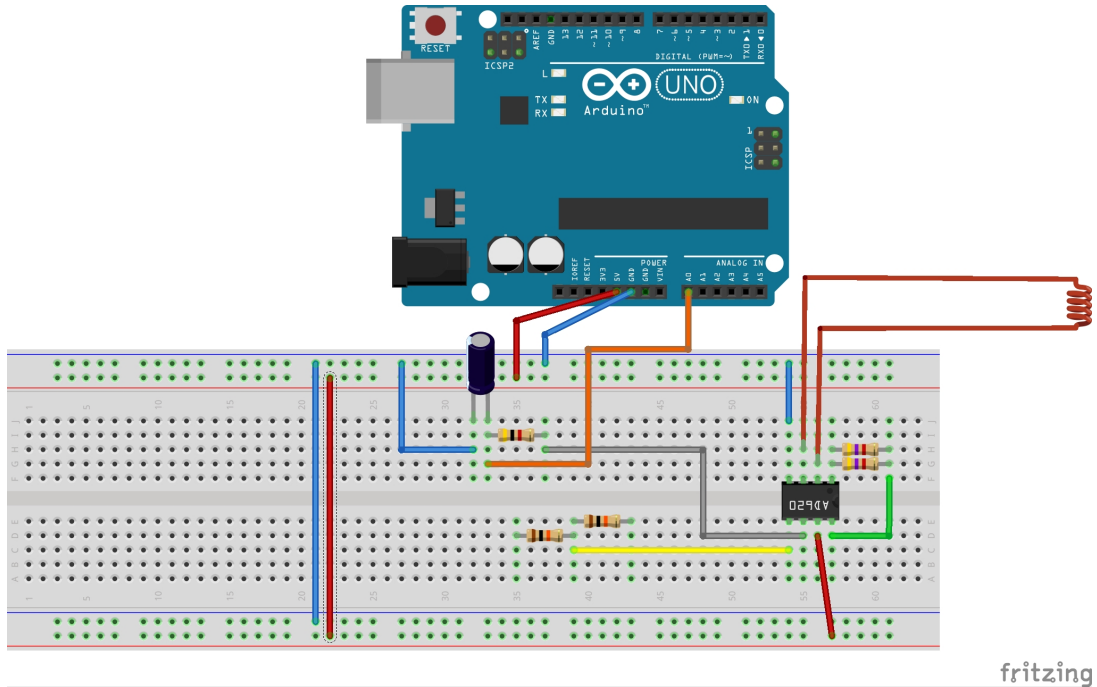


Figure 13: Complete circuit with AD620



### 5.3 Noise Analysis and RC Filter

Idle measurements showed a dominant interference near 100 Hz. To suppress this while preserving the 1–10 Hz vibration band, a first-order low-pass filter was placed after the offset stage with

$$\omega_c = 20 \text{ rad/s} \Rightarrow \omega_c = 2\pi f_c \approx 62.8 \text{ Hz}.$$

For a single-pole RC,

$$RC = \frac{1}{\omega_c} = \frac{1}{62.8}$$

The simplified schematic of the post-amp offset+RC network is shown in Fig. 14, and the full breadboard implementation in Fig. 13.

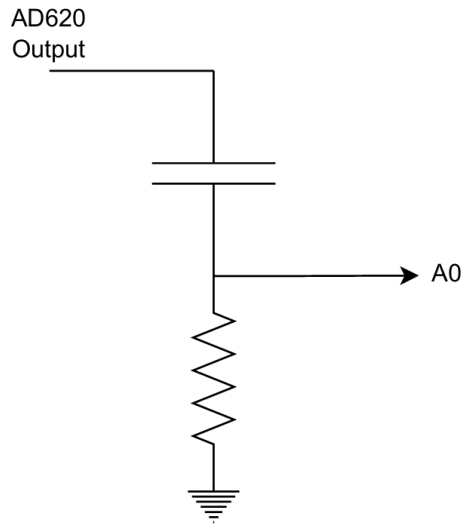


Figure 14: Post-amplifier DC offset and RC low-pass filter ( $\omega_c = 20 \text{ rad/s}$ ).

## 6 Calibration

### 6.1 DC Motor Method

The first method we considered for calibrating the coil-magnet system was the use of a direct current (DC) motor as a source of controlled periodic excitation. The concept behind this approach was straightforward: by attaching a small cam to the shaft of the motor, the rotational motion of the shaft could be transformed into a periodic contact or displacement of the ruler. The magnet attached to the free end of the ruler would then oscillate as the cam struck or displaced it, thereby inducing a corresponding voltage in the coil positioned below. The frequency of oscillation could in principle be directly related to the rotational speed of the motor, which is a well-defined and repeatable quantity. In theory, this method offered an attractive way to generate a known frequency of oscillation without relying on manual action or the natural resonance of the ruler itself.

In practice, the setup was constructed using the DC motor, which had a rated supply voltage of 12 V and a no-load speed of approximately 330 RPM. This corresponds to a rotational frequency of about 5.5 Hz. Unfortunately, a 12 V power supply was not available at the time of experimentation, and the only source we could access was a 5 V supply. This immediately placed a fundamental limitation on the system, as the motor could not operate at its rated speed or torque under the reduced voltage. As a result, the maximum achievable frequency in our tests was around 1.7 Hz. Moreover, once the cam was attached to the shaft, the additional load further reduced the effective rotational speed, lowering the RPM even more compared to the unloaded condition. While this frequency was sufficient to produce motion, it was far below the range we needed in order to test and calibrate the system more broadly. The reduced operational capacity of the motor was the first indication that this method might not be adequate for our purposes.



Figure 15: The motor used for calibration

#### 6.1.1 Experimental Setup and Procedure

The motor shaft was fitted with a small cam, fabricated from a lightweight material to minimize loading on the motor. The cam was designed to exert a periodic displacement on the ruler by striking or pushing its free end once during each rotation. The magnet was securely attached to the free end of the ruler, and the coil was placed beneath it. Each time the cam contacted the ruler, the magnet was displaced slightly, and the resulting oscillation generated a measurable voltage signal in the coil. These voltage signals were recorded using the Arduino, and the data was later analyzed in MATLAB using the Fast Fourier Transform (FFT) in order to identify the dominant oscillation frequency.

Initially, the setup appeared promising. The motor rotated consistently at its reduced speed, and the cam was able to make regular contact with the ruler. Voltage signals were successfully detected, and the FFT results showed peaks at frequencies close to the motor's speed. However, as the experiments

progressed, several serious issues became evident. These issues were not only practical inconveniences but also fundamental limitations that made the method unsuitable as a reliable calibration approach.

### 6.1.2 Observations and Problems

The first problem arose from the insufficient torque of the motor at 5 V. While the motor was capable of turning the cam, the motion was not smooth or uniform. At certain points in the rotation, the motor appeared to struggle to overcome the resistance introduced by the cam–ruler interaction. This caused irregularities in the displacement of the ruler and made the induced voltage signals less consistent than expected. A smooth and periodic excitation is essential for reliable calibration, but under these conditions the excitation was erratic and difficult to control.

A second and even more important issue was the introduction of electromagnetic interference. The DC motor is itself an electromagnetic device, and its operation generates both magnetic fields and electrical noise, particularly due to the brushes and commutator. Since our measurement system relied on detecting small voltages induced in a coil, the presence of a strong, fluctuating magnetic source so close to the coil inevitably contaminated the measurements. This interference manifested as background noise in the recorded signals, making it more challenging to isolate the true oscillation frequency of the magnet.

Another major difficulty was related to the mechanical nature of the excitation. Each time the cam struck the ruler, it did not simply displace the ruler at the intended frequency. Instead, the sudden impact generated a burst of high-frequency vibrations in the ruler, superimposed on the desired oscillatory motion. These vibrations were transmitted to the magnet and consequently appeared in the voltage signal as high-frequency noise components. When the FFT was applied, these bursts showed up as spurious peaks at higher frequencies, obscuring the main frequency of interest. In other words, rather than producing a clean periodic excitation, the motor–cam interaction introduced a combination of the desired fundamental frequency and an unwanted spectrum of higher-frequency vibrations. This made it very difficult to use the data for precise calibration.

In addition to these problems, the mechanical stability of the setup was far from ideal. The cam and ruler interaction was prone to misalignment, and repeated impacts caused wear and slight shifts in position over time. The result was a lack of repeatability: two trials performed under seemingly identical conditions could produce significantly different signal patterns. For a calibration method to be considered reliable, consistency is crucial, and this inconsistency rendered the motor approach unsuitable.

### Reasons for Unsuitability

Taken together, the problems encountered in the DC motor method can be summarized as follows:

- **Limited frequency range:** Because only a 5 V supply was available instead of the rated 12 V, the motor was unable to achieve its nominal speed of 330 RPM. In practice, the maximum frequency reached was only about 1.7 Hz. This narrow range was far below the desired calibration span, which meant that the motor could not be used to test higher frequency behavior. A calibration method that is restricted to such a low frequency range cannot provide the generality required for validating the measurement system.
- **Insufficient torque at reduced voltage:** The reduced supply voltage not only lowered the motor speed but also decreased its torque. As a result, the motor struggled to move the cam smoothly, especially when it came into contact with the ruler. Instead of a steady periodic displacement, the motion became irregular and jerky. This irregularity transferred directly into the induced signals, making them inconsistent and unreliable for precise FFT analysis. The inability to provide a stable excitation is a critical drawback for calibration purposes.
- **Electromagnetic interference from the motor:** The DC motor itself is an active electromagnetic device, containing both permanent magnets and a commutator–brush assembly. During

operation, it generates fluctuating magnetic fields and electrical noise that spread into the surrounding environment. Since our measurement principle relied on detecting very small induced voltages in the coil, the proximity of the motor created a significant source of interference. The recorded signals therefore contained background noise unrelated to the magnet's motion, reducing the clarity and trustworthiness of the results.

- **High-frequency vibration bursts after cam impact:** Perhaps the most serious problem was caused by the mechanical impact of the cam on the ruler. Each time the cam touched the ruler, the contact did not only introduce the desired displacement but also excited a burst of high-frequency vibrations in the ruler. These vibrations propagated through the magnet and into the induced voltage signal. In the FFT, they appeared as spurious peaks at much higher frequencies than the fundamental oscillation. This noise masked the true frequency content and made it extremely difficult to isolate the main peak. Instead of clean frequency data, the result was a spectrum cluttered with unwanted components.
- **Mechanical instability and poor repeatability:** The interaction between the cam and the ruler depended heavily on alignment and contact geometry. Even small shifts during operation caused noticeable differences in the way the cam struck the ruler. Over repeated trials, the impacts became inconsistent due to mechanical wear and looseness in the setup. A calibration method must be stable and repeatable if it is to be trusted, but the motor method exhibited neither of these qualities. The lack of consistency meant that even at the same speed setting, the recorded signals varied significantly, which is unacceptable for a calibration standard.

In summary, while the motor method initially appeared practical, the combination of these problems made it unsuitable as a reliable calibration technique. Each issue alone would have posed difficulties, but together they eliminated the possibility of obtaining clear and accurate frequency measurements.

### 6.1.3 Conclusion on DC Motor Method

Although the DC motor method seemed attractive in principle, offering the promise of a controllable and repeatable excitation source, the experimental reality fell far short of expectations. The reduced frequency range, insufficient torque, electromagnetic interference, high-frequency noise bursts, and poor mechanical stability meant that the method could not deliver the reliable calibration data that we required. In practice, the motor method yielded only a single usable calibration point at approximately 1.7 Hz, and even that point was affected by noise and irregularities. For this reason, the DC motor method was ultimately set aside in favor of the metronome and ruler methods, both of which offered greater accuracy, consistency, and suitability for our project. The results of this method, including the induced voltage versus time and the corresponding FFT spectrum, are shown in the Figure ?? and Figure 17 below.

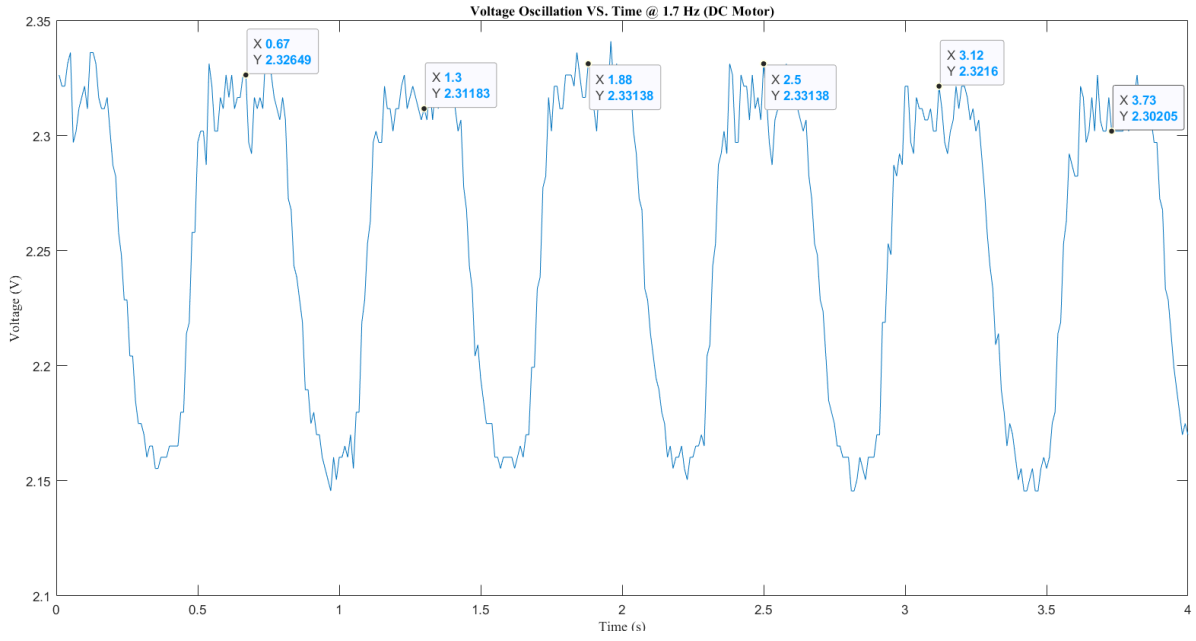


Figure 16: The motor used for calibration

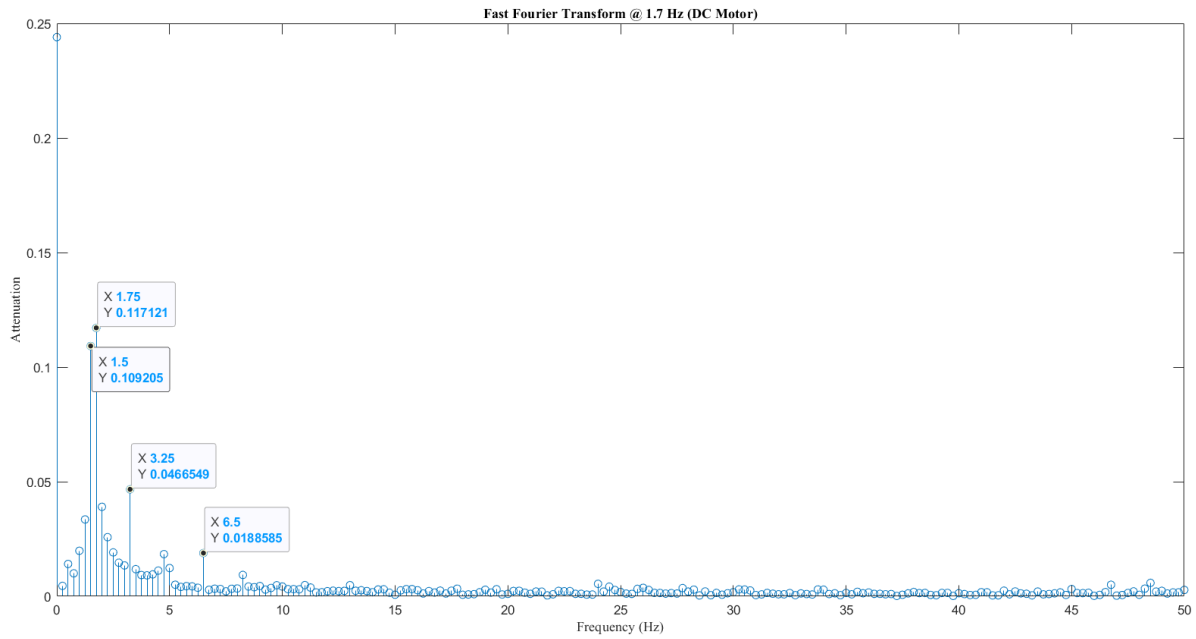


Figure 17: FFT result of calibration with DC motor

As shown in the figure, the FFT result clearly indicates a dominant peak at approximately 1.75 Hz, which is in very close agreement with the expected excitation frequency of 1.7 Hz. The additional leakage and smaller side peaks observed in the spectrum are attributed to the noise sources and high-frequency vibrations previously discussed.

## 6.2 Metronome Method

After the limitations of the DC motor approach became clear, a second calibration strategy was developed based on the use of a mechanical metronome. The idea was to employ the metronome as a reliable and externally controlled frequency source. Unlike the motor, which suffered from power supply issues and mechanical noise, the metronome could produce clean and repeatable beats at a wide range of frequencies within the low-frequency domain. By synchronizing the manual motion of the magnet with the ticking of the metronome, we were able to excite the ruler and coil system at precisely known frequencies and then record the induced voltages for analysis.

### Setup and Procedure

A metronome application was placed on the table next to the experimental setup, and its frequency per minute was adjusted to predefined beats per second, corresponding to the frequencies of interest. The metronome picture is shown in Figure 18 below, which illustrates the exact device used in our calibration procedure. Once the metronome was set to a desired frequency, for example 1 Hz or 4 Hz, the operator manually oscillated the magnet in and out of the coil in rhythm with the audible clicks of the metronome. The Arduino was used to acquire the voltage signals induced in the coil, and the data was subsequently transferred to MATLAB for FFT analysis.

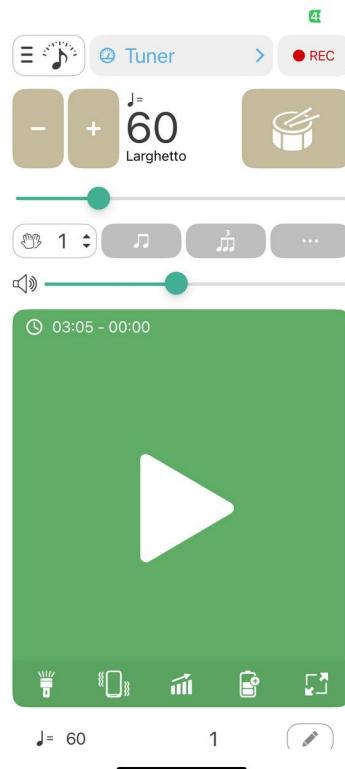


Figure 18: Metronome application set to 60 times per minutes which means 1 Hz

The manual synchronization between the hand movement and the metronome was effective. At low frequencies, the human response time was sufficient to match the beat with high accuracy. This allowed us to generate clean, periodic oscillations of the magnet relative to the coil. The resulting signals, both in the time domain and in the frequency domain, confirmed that the metronome method was capable of producing reliable calibration data. As an example the results for two different frequencies are shown.

## Results at 1 Hz

The first test was conducted at 1 Hz, corresponding to one full oscillation per second. Figure 19 shows the induced voltage as a function of time at this frequency. The signal exhibits a clear periodicity, with successive peaks and troughs occurring at regular intervals of approximately one second. The amplitude of the signal was stable and consistent across the duration of the measurement, which demonstrates the effectiveness of the metronome in guiding the excitation.

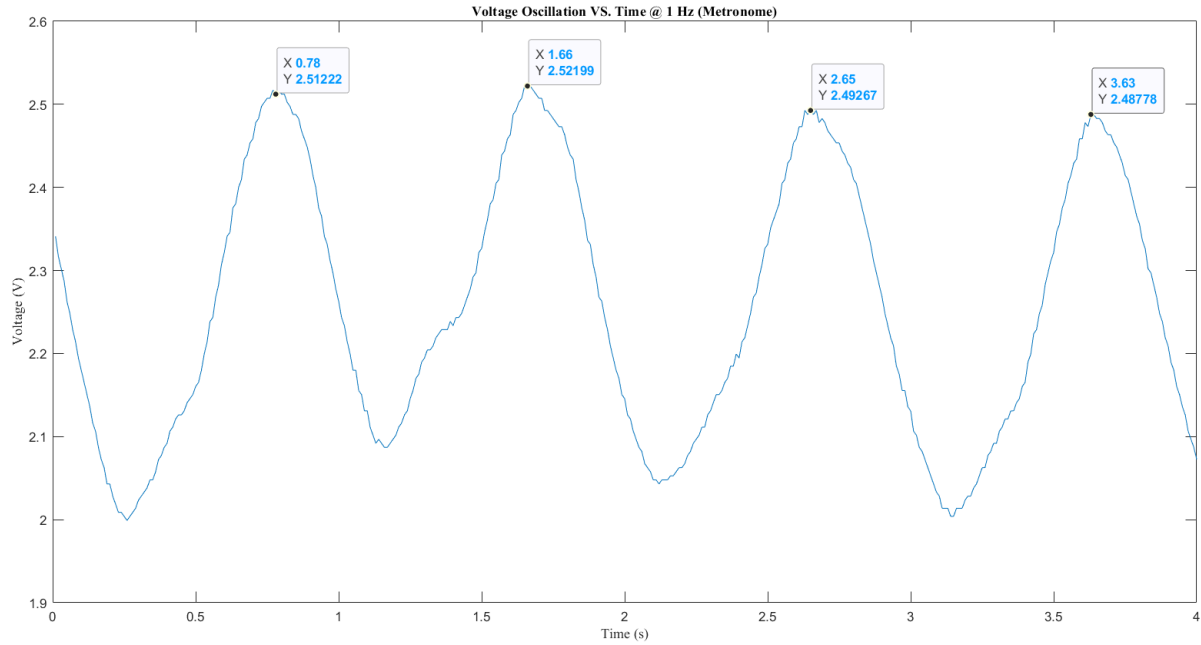


Figure 19: Voltage induced in the coil vs time at 1 Hz (metronome)

The FFT of the 1 Hz signal is presented in Figure ???. As can be seen, there is a sharp and dominant peak at 1 Hz, which perfectly corresponds to the set frequency of the metronome. The presence of this peak confirms that the system is able to correctly capture and reflect the true oscillation frequency of the magnet. Minor spectral leakage can also be observed around the main peak, but this effect is expected due to the finite length of the data window and the imperfect manual excitation. The leakage did not interfere with the ability to identify the correct fundamental frequency.



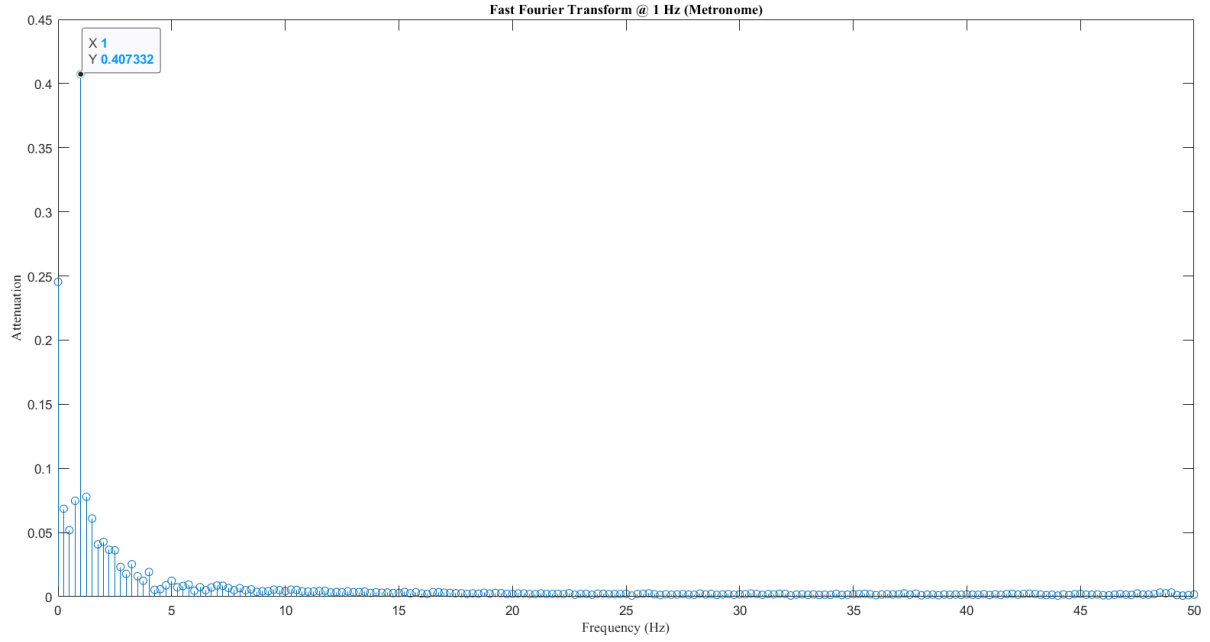


Figure 20: FFT results for 1 Hz induced voltage (metronome)

## Results at 4 Hz

To further validate the method at a higher frequency, the metronome was set to 4 Hz, and the same procedure was repeated. Figure 21 Figure 22 shows the FFT result for this case. Once again, a sharp peak is visible at 4 Hz, closely matching the set frequency of the metronome. Although the manual motion was more demanding at this higher frequency, the operator was able to maintain sufficient synchronization with the beat to ensure reliable results. The FFT spectrum shows slightly more leakage and small side peaks compared to the 1 Hz case, which is consistent with the increased difficulty of producing perfectly regular hand movements at higher speed. Nevertheless, the dominant peak at 4 Hz is unambiguous and confirms the accuracy of the method.

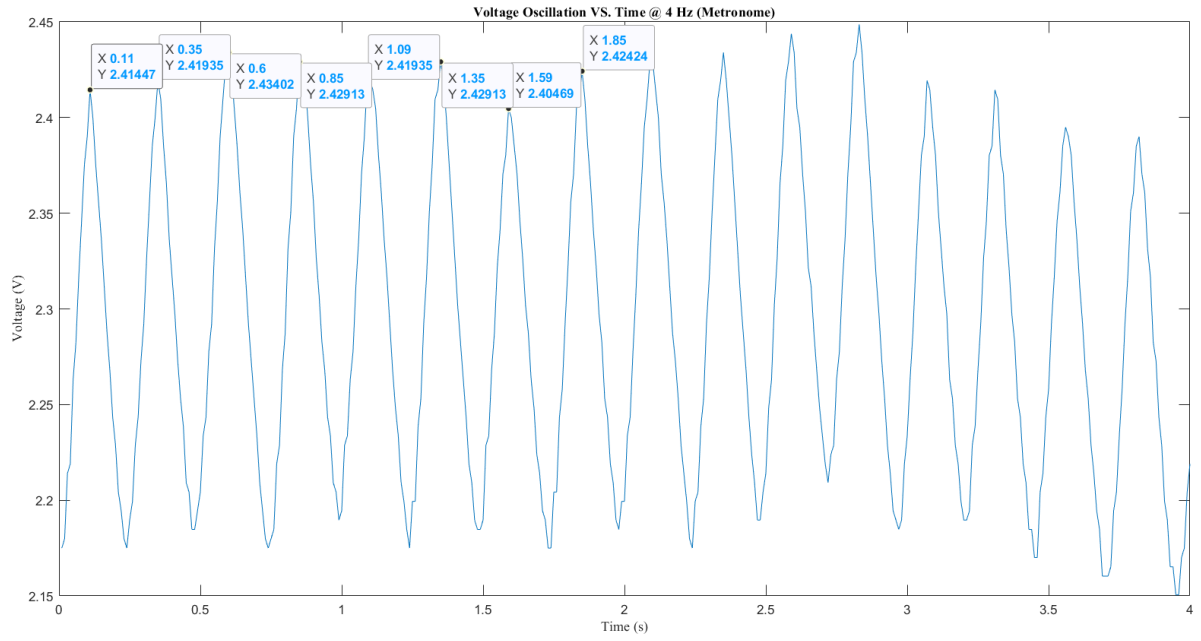


Figure 21: Voltage induced in the coil vs time at 4 Hz (metronome)

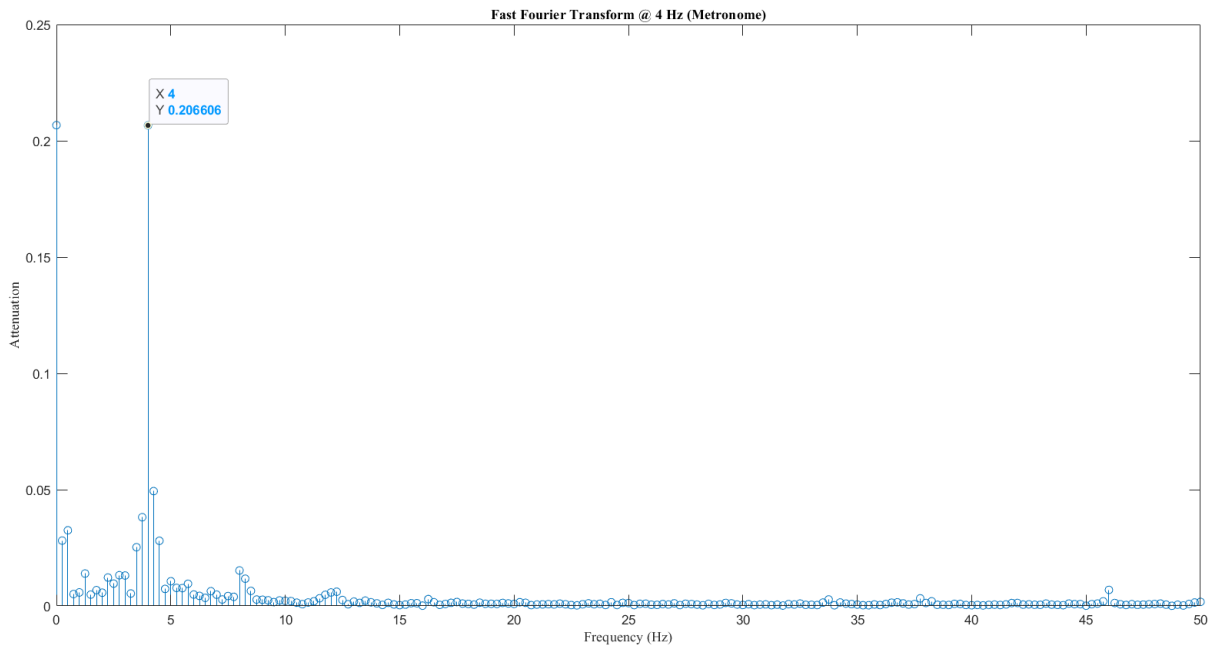


Figure 22: FFT results for 4 Hz induced voltage with (metronome)

## Strengths and Limitations

The metronome method provided several advantages compared to the DC motor method. Most importantly, it offered a clean and easily adjustable reference frequency that could be set with confidence by simply moving the sliding weight of the metronome arm. The human operator was able to synchronize motion with the audible clicks, and the results showed excellent agreement between the set frequency and the FFT outcomes. The time-domain signals were also clean and stable, indicating that this method

produced high-quality excitation without the interference issues associated with the motor.

However, the method was not without its limitations. The most obvious drawback was the restriction to relatively low frequencies. In practice, it was only feasible to maintain synchronization up to about 5 Hz, beyond which the manual motion became too fast and irregular. While this range was sufficient to demonstrate the accuracy of the setup in the low-frequency domain, it could not provide calibration data for higher-frequency vibrations. Another limitation was the reliance on the operator's consistency. Small variations in hand motion, even while following the beat, introduced minor irregularities into the signal. These irregularities manifested as spectral leakage in the FFT, though they did not prevent identification of the fundamental frequency.

Despite its limitations, the metronome method proved to be a powerful tool for initial calibration. The results at both 1 Hz and 4 Hz showed close agreement between the expected and measured frequencies. The method was simple to implement, required no additional power supplies or mechanical fabrication, and avoided the electromagnetic noise problems of the DC motor. For these reasons, it played an important role in establishing confidence in the measurement system during the early stages of the project.

The combination of clean time-domain signals, sharp FFT peaks, and straightforward operation makes the metronome method an excellent baseline calibration approach. Although it cannot be extended to higher frequencies, its accuracy within the 1–5 Hz range provided a solid reference against which other methods could be compared.

## 6.3 Ruler Method

The third and final calibration strategy, which ultimately became the main method of reference, was based on the natural frequency of a cantilevered metal ruler. This approach was selected after the limitations of both the DC motor and metronome methods became clear. The motor lacked stability and introduced unwanted noise, while the metronome was restricted to low frequencies. In contrast, the cantilevered ruler offered a simple yet effective way of generating a wide range of natural frequencies by varying the free length of the ruler that extended beyond the table edge. By exciting the ruler with an initial displacement and letting it vibrate freely, we obtained clean oscillations that could be measured and analyzed. Because the vibration frequency of a cantilever beam is well understood theoretically, it was possible to directly compare experimental results with analytical predictions.

### Setup and Procedure

The experimental setup for this method is shown in the Figure 23. One end of the ruler was fixed to the table by hand, while the remaining part of the ruler was allowed to hang freely in the air. A permanent magnet was attached to the free end of the ruler, and a coil was positioned directly beneath the magnet. When the ruler was given a small jerk and released, it entered free vibration. The oscillatory motion of the magnet induced a voltage in the coil, which was measured and recorded using the Arduino. The recorded time-domain signals were then analyzed in MATLAB using FFT to determine the dominant frequency of oscillation.

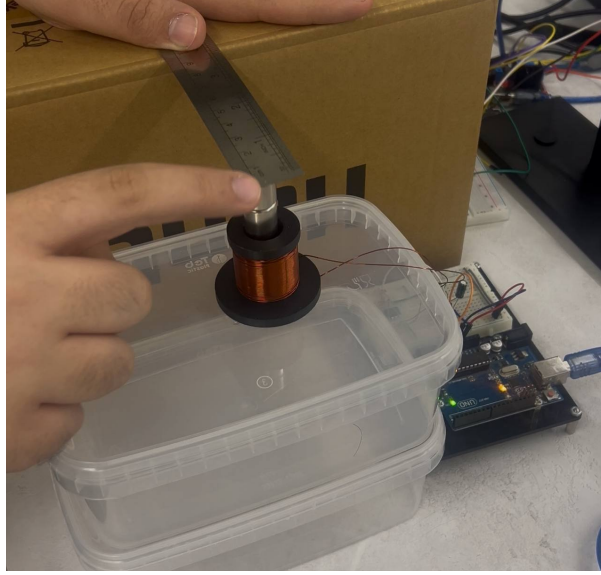


Figure 23: The setup for calibration with natural frequency of the ruler

An important advantage of this method was the ability to vary the effective length of the ruler that extended beyond the table edge. By increasing or decreasing the free length, the stiffness of the cantilever changed, which directly affected its natural frequency. Shorter free lengths produced higher natural frequencies, while longer free lengths resulted in lower frequencies. This allowed us to span a wide range of calibration points using a single physical setup.

## Theoretical Background

The natural frequency of a cantilever beam with an attached tip mass can be estimated using classical vibration theory. The fundamental mode frequency depends on the material properties (elastic modulus and density), geometric dimensions (width, thickness, and length), and the effective tip mass. In our case, the ruler itself served as the beam, and the attached magnet acted as the tip mass. While exact analytical modeling is complex, standard formulas provided reliable estimates for the expected frequencies at different free lengths. The following values of free length and corresponding theoretical natural frequencies were calculated:

Table 1: Experimental results for ruler natural frequencies at different free lengths.

Free length of ruler (cm)	Theoretical frequency (Hz)
6	17.719
7	14.164
10	8.355
11	7.243
13	5.631
14	5.033
16	4.109
19	3.160

## Experimental Results

The experimental results for this method are illustrated with several examples. When the free length of the ruler was set to 7 cm, the induced voltage signal recorded at this condition is shown in Figure 24, while the FFT analysis is presented in Figure 25. The time-domain waveform demonstrates clear periodic oscillations, and the frequency spectrum exhibits a sharp peak at the dominant frequency.

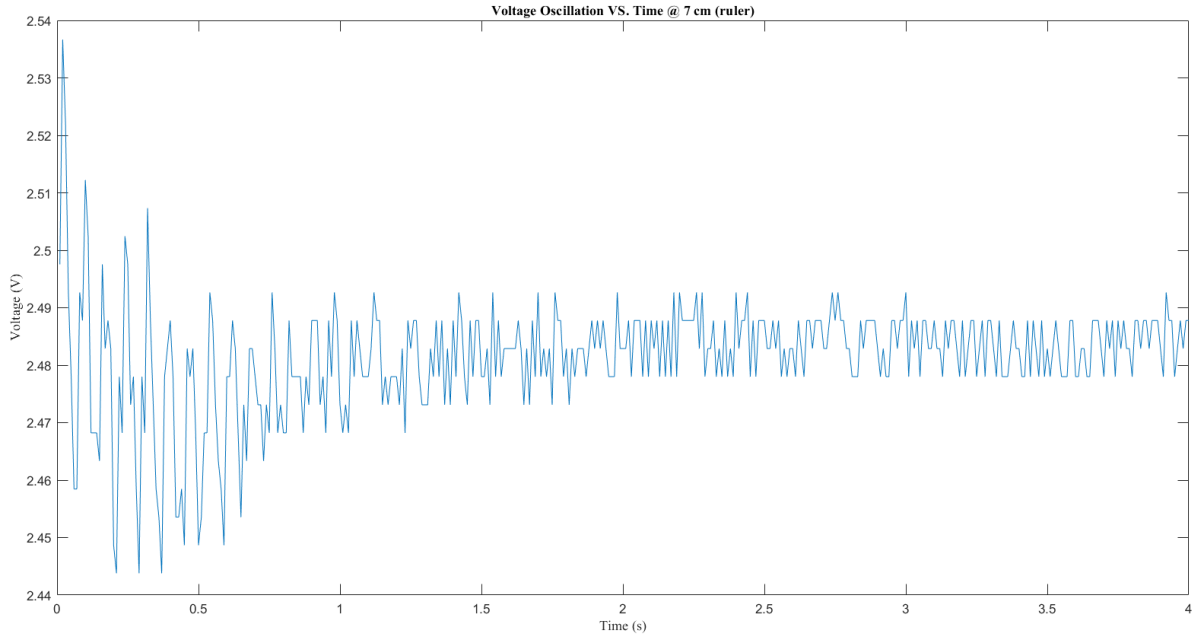


Figure 24: Induced voltage signal for 7 cm free length of the ruler

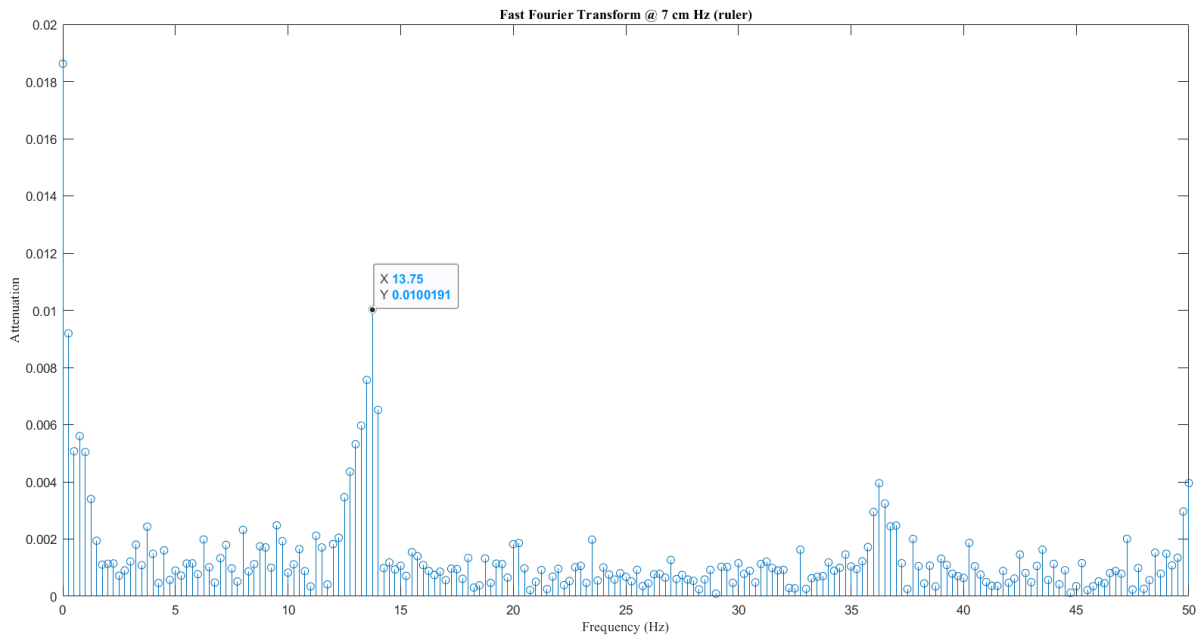


Figure 25: FFT spectrum for 7 cm free length of the ruler

A second example was conducted at a free length of 11 cm. The induced voltage signal for this case is shown in Figure 26, and its FFT is provided in Figure 27. These results present the typical response of the system when the ruler length was adjusted to this configuration.

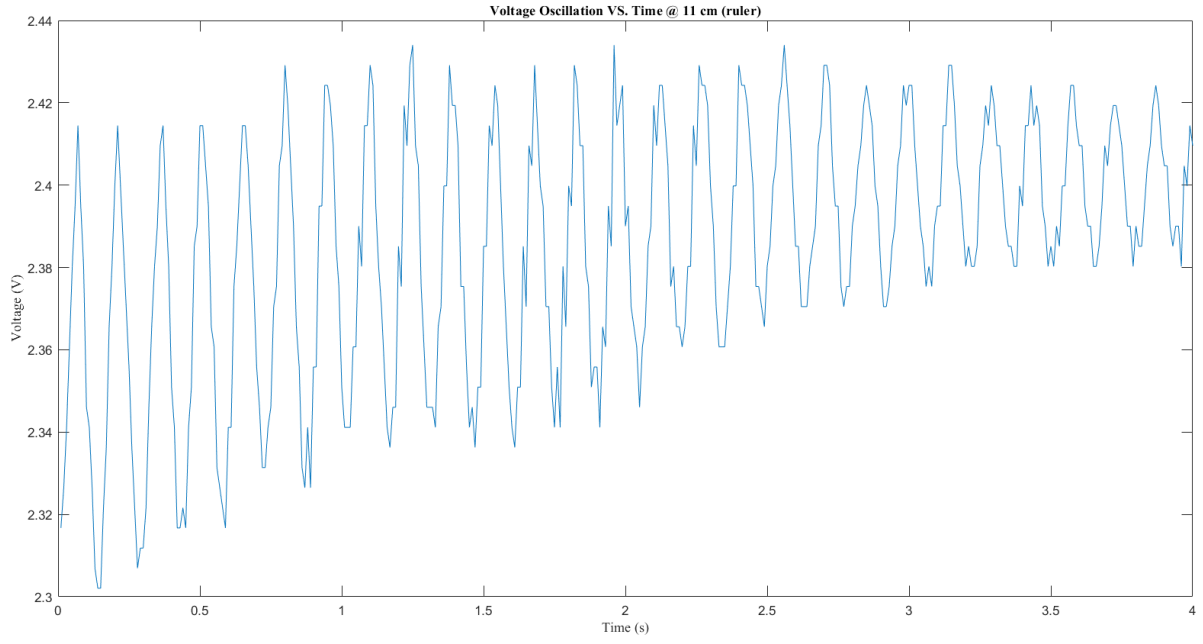


Figure 26: Induced voltage signal for 11 cm free length of the ruler

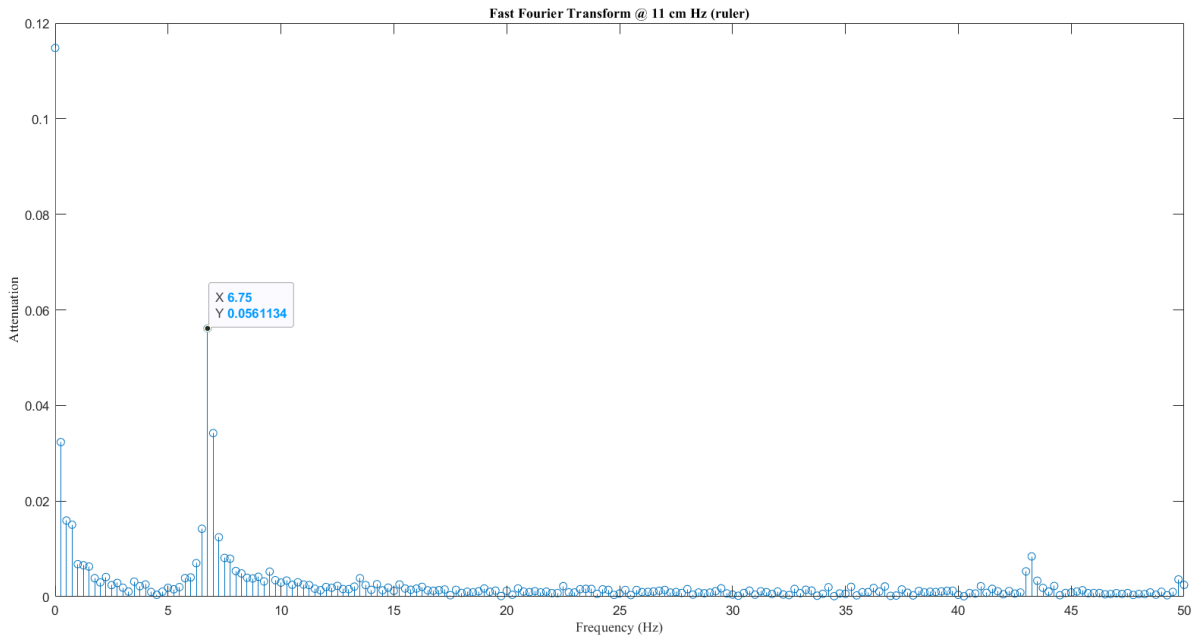


Figure 27: FFT spectrum for 11 cm free length of the ruler

To further illustrate the performance of this method at even lower frequencies, a third example was conducted at a free length of 16 cm. Figure 28 and 29 present the induced voltage and the FFT spectrum for this case. Although the signal amplitude was somewhat reduced due to the lower stiffness of the ruler, the frequency content remained distinct and measurable.

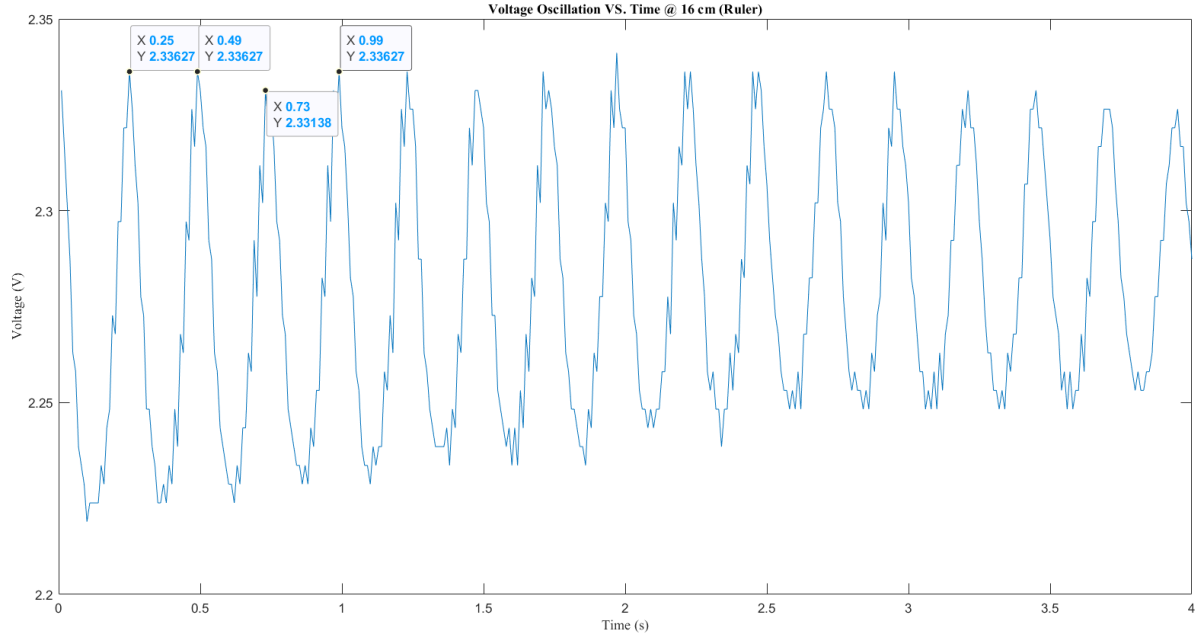


Figure 28: Induced voltage signal for 16 cm free length of the ruler

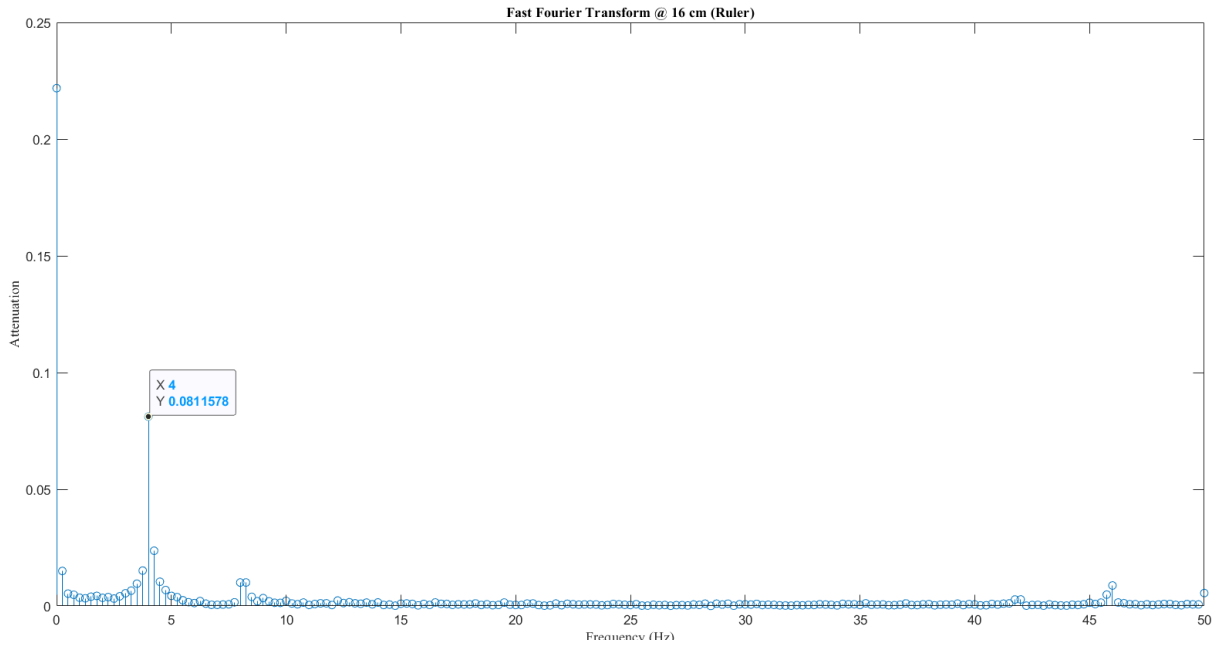


Figure 29: FFT spectrum for 16 cm free length of the ruler

## Discussion

These three representative cases (7 cm, 11 cm, and 16 cm) demonstrate the robustness of the ruler calibration method. The ability to tune the frequency simply by changing the free length of the ruler made this approach highly flexible. Moreover, the oscillations were clean and free of the electromagnetic interference problems encountered with the motor method. Compared to the metronome, the ruler offered a much broader frequency range, extending from around 3 Hz up to nearly 18 Hz in our experiments.

This allowed us to calibrate the coil–magnet system across a significantly wider operating spectrum.

It is also worth noting that although minor spectral leakage was present in some FFT plots, the dominant peaks corresponding to the natural frequencies were always clearly visible. This indicates that the system not only provided accurate frequency values but also maintained good signal-to-noise ratios, which is essential for reliable calibration. The close match between theoretical predictions and experimental outcomes further reinforced the credibility of this method. In practice, only very small adjustments were necessary to align the experimental frequencies with the analytical values.

In conclusion, the ruler method proved to be the most effective and versatile of all three calibration strategies tested. The setup was simple, the results were consistent, and the agreement with theory was good. By systematically varying the free length of the ruler, a wide range of natural frequencies could be explored, providing a comprehensive calibration basis for the coil–magnet measurement system. The time-domain signals and FFT results at 7 cm, 11 cm, and 16 cm serve as representative examples of the method’s accuracy. Given these strengths, the ruler-based approach was selected as the primary calibration technique for the remainder of the project.

## 6.4 Theory: Natural Frequency of the Cantilevered Ruler with a Tip Magnet (and Rotary Inertia)

### Beam Governing Equation

Under the assumption of small transverse deflections, the vibration of the ruler can be modeled using the Euler–Bernoulli beam theory. The transverse displacement is denoted by  $w(x, t)$ , where  $x$  is the coordinate along the beam length ( $0 \leq x \leq L$ ), and  $t$  is time. The governing partial differential equation (PDE) for free vibration is

$$EI \frac{\partial^4 w}{\partial x^4}(x, t) + \rho A \frac{\partial^2 w}{\partial t^2}(x, t) = 0, \quad 0 < x < L. \quad (1)$$

Here:

- $E$  is the Young’s modulus of the beam material (a measure of stiffness).
- $I = \frac{bt^3}{12}$  is the second moment of area of the beam’s cross-section (resistance to bending).
- $\rho$  is the density of the beam material.
- $A = bt$  is the cross-sectional area of the beam (width  $b$  times thickness  $t$ ).
- $w(x, t)$  is the transverse deflection of the beam at position  $x$  and time  $t$ .

The boundary conditions are:

- At the clamped end ( $x = 0$ ):  $w(0, t) = 0$  and  $\frac{\partial w}{\partial x}(0, t) = 0$  (no deflection, no slope).
- At the free end ( $x = L$ ):  $\frac{\partial^2 w}{\partial x^2}(L, t) = 0$  and  $\frac{\partial^3 w}{\partial x^3}(L, t) = 0$  (no bending moment, no shear force).

### Reduction to a Single Degree of Freedom (Tip Motion)

For calibration purposes, we are mainly interested in the first (fundamental) mode of vibration, which dominates the response. To simplify, we approximate the beam as a single degree of freedom system by tracking only the displacement at the free end:

$$q(t) := w(L, t),$$



where  $q(t)$  is the tip deflection. The actual beam motion can then be written as  $w(x, t) = \phi(x)q(t)$ , where  $\phi(x)$  is the fundamental mode shape normalized such that  $\phi(L) = 1$  (so at the tip,  $w(L, t) = q(t)$ ).

In this reduced model:

$$k_{\text{tip}} = \frac{F}{\delta_{\text{tip}}} = \frac{3EI}{L^3}, \quad (2)$$

$$m_{\text{beam,eff}} = \alpha \rho AL, \quad \alpha \approx 0.236, \quad (3)$$

where:

- $k_{\text{tip}}$  is the effective stiffness of the beam as seen from the tip. It comes from the static deflection formula  $\delta_{\text{tip}} = FL^3/(3EI)$  for a tip load  $F$ .
- $m_{\text{beam,eff}}$  is the effective modal mass of the beam that contributes to the tip motion.
- $\alpha \approx 0.236$  is a constant for the first vibration mode of a cantilever beam, obtained by integrating the squared mode shape  $\phi(x)$ .

### Effect of Tip Mass and Rotary Inertia

At the free end, a magnet assembly is attached. Its contribution is twofold:

1. A **translational tip mass**,  $M_t$ , equal to the combined mass of the two cylindrical magnets.
2. A **rotational inertia** due to the finite size of the magnets. When the beam vibrates, the free end not only translates but also rotates slightly.

Let  $\theta(t)$  denote the rotation of the tip (slope of the beam at  $x = L$ ). Since  $w(x, t) = \phi(x)q(t)$ , the slope at the tip is

$$\theta(t) = \phi'(L)q(t) = \frac{\kappa}{L}q(t), \quad (4)$$

where  $\kappa = L \frac{\phi'(L)}{\phi(L)} \approx 1.377$  is a dimensionless constant for the first mode of a cantilever beam.

If the magnet assembly has a mass moment of inertia  $J$  about its centroid (perpendicular to the bending plane), its rotational kinetic energy is

$$T_{\text{rot}} = \frac{1}{2}J\dot{\theta}^2.$$

This is equivalent to adding an effective mass term at the tip:

$$m_{\text{rot}} = \frac{J\kappa^2}{L^2}. \quad (5)$$

Here:

- $J$  depends on the geometry of the magnet. For a cylinder of mass  $M_t$ , radius  $r = d/2$ , and height  $h_{\text{tot}} = 2h$ , the moment of inertia about a centroidal axis perpendicular to its axis of symmetry is

$$J = \frac{1}{12}M_t(3r^2 + h_{\text{tot}}^2).$$

- $m_{\text{rot}}$  is the equivalent added mass due to rotation, projected onto the tip motion coordinate.

## Effective Model

Collecting all contributions, the equivalent single-degree-of-freedom model for the ruler with tip magnet is:

$$m_{\text{eff}} \ddot{q}(t) + k_{\text{tip}} q(t) = 0, \quad (6)$$

where

$$m_{\text{eff}} = M_t + m_{\text{beam,eff}} + m_{\text{rot}}.$$

The natural frequency is then

$$\omega_n = \sqrt{\frac{k_{\text{tip}}}{m_{\text{eff}}}}, \quad f = \frac{\omega_n}{2\pi}. \quad (7)$$

**Tip magnet mass and rotary inertia.** Each magnet is a solid cylinder of density  $\rho_{\text{mag}}$ , diameter  $d$  (radius  $r = d/2$ ), and height  $h$ . Its mass is

$$m_1 = \rho_{\text{mag}} \left( \frac{\pi d^2}{4} h \right). \quad (8)$$

With two identical magnets *axially stacked end-to-end*, we treat them as a single cylinder of height  $h_{\text{tot}} = 2h$  and total mass  $M_t = 2m_1$ . The mass moment of inertia of a solid cylinder about an axis through its centroid and *perpendicular* to the cylinder axis is

$$J = \frac{1}{12} M_t (3r^2 + h_{\text{tot}}^2). \quad (9)$$

**Effective single-DOF model and natural frequency.** Collecting contributions in the tip coordinate  $q(t)$ , the equivalent SDOF equation is

$$\underbrace{(M_t + m_{\text{beam,eff}} + m_{\text{rot}})}_{m_{\text{eff}}} \ddot{q}(t) + \underbrace{k_{\text{tip}}}_{\frac{3EI}{L^3}} q(t) = 0, \quad (10)$$

so the undamped natural circular frequency and frequency are

$$\omega_n = \sqrt{\frac{k_{\text{tip}}}{m_{\text{eff}}}} = \sqrt{\frac{\frac{3EI}{L^3}}{M_t + \alpha \rho AL + \frac{J\kappa^2}{L^2}}}, \quad f = \frac{\omega_n}{2\pi}. \quad (11)$$

**Parameters (as used in the computations).**

$$\begin{aligned} E &= 193 \times 10^9 \text{ Pa}, \quad \rho = 7850 \text{ kg/m}^3, \quad b = 26 \text{ mm}, \quad t = 0.5 \text{ mm}, \\ \rho_{\text{mag}} &= 7500 \text{ kg/m}^3, \quad d = 15 \text{ mm}, \quad h = 20 \text{ mm}, \quad \alpha = 0.236, \quad \kappa = 1.377. \end{aligned}$$

**Worked Example:**  $L = 11 \text{ cm}$

For a free length  $L = 0.11 \text{ m}$ :

**Beam section properties.**

$$A = bt = (0.026)(0.0005) = 1.30 \times 10^{-5} \text{ m}^2, \quad I = \frac{bt^3}{12} = \frac{0.026(0.0005)^3}{12} = 2.7083 \times 10^{-13} \text{ m}^4.$$

**Tip stiffness.**

$$k_{\text{tip}} = \frac{3EI}{L^3} = \frac{3(193 \times 10^9)(2.7083 \times 10^{-13})}{(0.11)^3} = 1.1782 \times 10^2 \text{ N/m.}$$

**Magnet mass and rotary inertia.** One magnet mass:

$$m_1 = \rho_{\text{mag}} \left( \frac{\pi d^2}{4} h \right) = 7500 \left( \frac{\pi(0.015)^2}{4} \cdot 0.020 \right) = 2.6507 \times 10^{-2} \text{ kg.}$$

Two magnets (stacked):  $M_t = 2m_1 = 5.3014 \times 10^{-2} \text{ kg}$ . Treating them as a single cylinder of height  $h_{\text{tot}} = 0.040 \text{ m}$  and radius  $r = 0.0075 \text{ m}$ :

$$J = \frac{1}{12} M_t (3r^2 + h_{\text{tot}}^2) = \frac{1}{12} (0.053014) (3(0.0075)^2 + (0.040)^2) = 7.8141 \times 10^{-6} \text{ kg} \cdot \text{m}^2.$$

Equivalent translational (rotary) mass in the tip coordinate:

$$m_{\text{rot}} = \frac{J\kappa^2}{L^2} = \frac{(7.8141 \times 10^{-6})(1.377)^2}{(0.11)^2} = 1.2245 \times 10^{-3} \text{ kg.}$$

**Beam effective (modal) mass at the tip.** Total beam mass over  $L$ :

$$m_{\text{beam}} = \rho AL = (7850)(1.30 \times 10^{-5})(0.11) = 1.12255 \times 10^{-2} \text{ kg.}$$

Effective tip mass of the beam (mode 1 with  $\phi(L) = 1$ ):

$$m_{\text{beam,eff}} = \alpha m_{\text{beam}} = (0.236)(1.12255 \times 10^{-2}) = 2.6492 \times 10^{-3} \text{ kg.}$$

**Effective mass and frequency.**

$$m_{\text{eff}} = M_t + m_{\text{beam,eff}} + m_{\text{rot}} = (0.053014) + (0.0026492) + (0.0012245) = 5.6888 \times 10^{-2} \text{ kg.}$$

$$\omega_n = \sqrt{\frac{k_{\text{tip}}}{m_{\text{eff}}}} = \sqrt{\frac{117.82}{0.056888}} = 45.487 \text{ rad/s,} \quad f = \frac{\omega_n}{2\pi} = \boxed{7.243 \text{ Hz}}.$$

**Remarks.** Equation (11) shows how the frequency scales with length, stiffness, and end mass:  $f \propto L^{-3/2}$  via  $k_{\text{tip}} \propto L^{-3}$ , while  $m_{\text{eff}}$  increases with  $L$  through the beam's effective mass and decreases with  $L$  in the rotary term  $J\kappa^2/L^2$ . In our geometry, the tip mass  $M_t$  (two stacked cylindrical magnets) dominates  $m_{\text{eff}}$ , but both the beam modal mass ( $0.236 \rho AL$ ) and the rotary contribution  $J\kappa^2/L^2$  are non-negligible and are required for the correct frequency prediction.

## 6.5 Curve Fitting and Calibration Curve

After obtaining both theoretical predictions and experimental measurements of the natural frequencies of the ruler at different free lengths, a calibration step was required to establish a direct mathematical relationship between the two sets of results. The motivation was that the theoretical model, although based on beam vibration theory, contained approximations and assumptions (such as ideal boundary conditions and simplified mass distribution). On the other hand, the experimental results were affected by measurement errors, noise, and imperfections in the setup. A calibration curve therefore allows us to reconcile these two sources of data and to obtain a practical formula that directly converts theoretical predictions into experimentally observed values.

Table 2: Theoretical and experimental frequencies for different free lengths of the ruler.

Free length (cm)	$f_{\text{formula}}$ (Hz)	$f_{\text{measured}}$ (Hz)
6	17.719	18.00
7	14.164	13.75
10	8.355	8.00
11	7.243	6.75
13	5.631	5.50
14	5.033	4.50
16	4.109	4.00
19	3.160	3.25

### Data Used for Fitting

The data points used for curve fitting are summarized in Table 2. The column *ruler\_cm* shows the free length of the ruler in centimeters,  $f_{\text{formula}}$  is the theoretical frequency calculated from the beam-mass model, and  $f_{\text{measured}}$  is the frequency obtained experimentally from the FFT analysis.

### Fitting Procedure

The fitting was carried out using the MATLAB Curve Fitter toolbox. The theoretical frequencies  $f_{\text{formula}}$  were used as the independent variable ( $x$ -data), and the experimental frequencies  $f_{\text{measured}}$  were used as the dependent variable ( $y$ -data). A first-order polynomial (linear model) of the form

$$y = ax + b$$

was chosen, as it provides the simplest calibration relationship between theory and experiment. The fitting result is shown in Figure 30, which illustrates the alignment between the experimental data points and the fitted line. The final plot generated from MATLAB is shown in Figure 31.

### Results of Curve Fitting

The fitted calibration curve was found to be

$$f_{\text{measured}} = 1.0140 f_{\text{formula}} - 0.3224. \quad (12)$$

Here:

- The slope ( $a = 1.0140$ ) is very close to unity, indicating that the theoretical predictions closely follow the trend of the experimental values.
- The intercept ( $b = -0.3224$ ) is small, showing that there is only a slight systematic offset between the two datasets.

The quality of the fit was quantified by the coefficient of determination  $R^2 = 0.9971$ , which indicates an excellent match between the fitted line and the data points. The root mean squared error (RMSE) was 0.305, confirming that the deviations are very small.

### Discussion

The calibration curve demonstrates that the theoretical model provides an excellent estimate of the ruler's natural frequency, with only minor systematic deviation from the experimental values. The near-unity slope confirms that the fundamental trend of the theory is accurate, while the small negative intercept

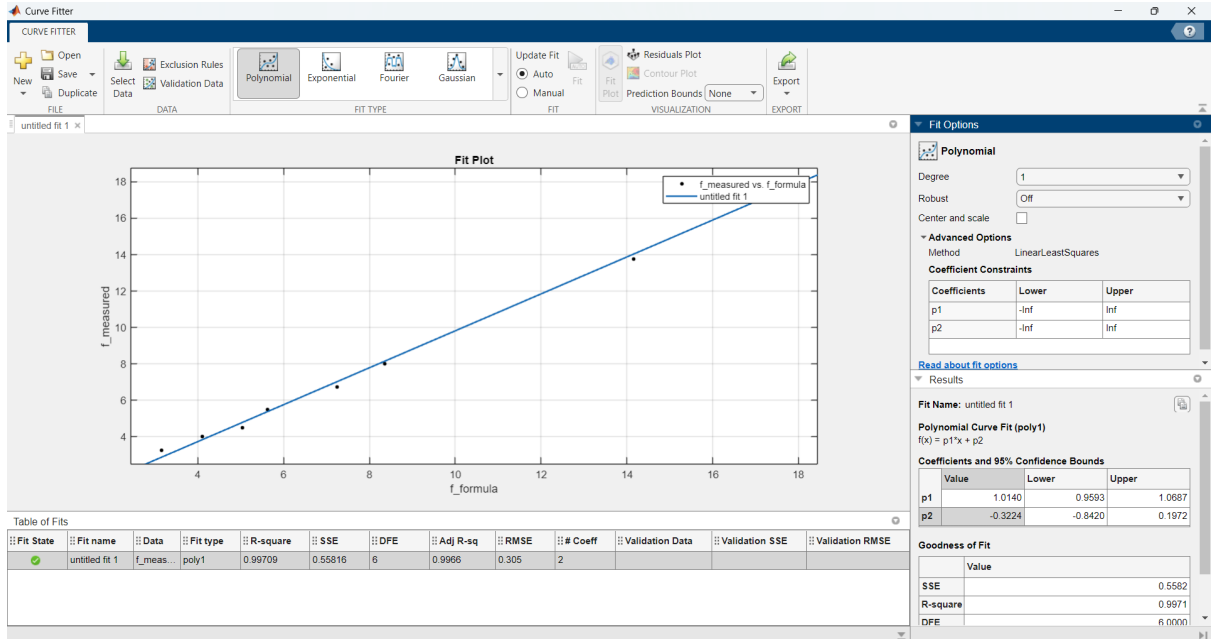


Figure 30: Curve fitting performed in MATLAB Curve Fitter:  $f_{\text{measured}}$  vs.  $f_{\text{formula}}$ .

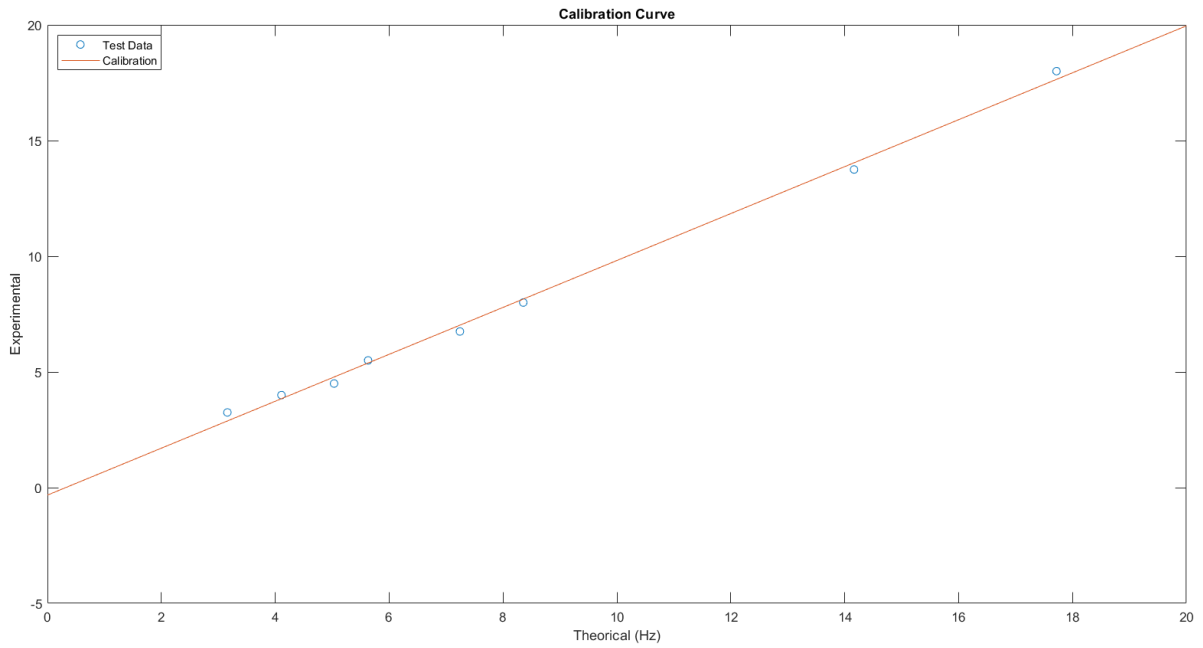


Figure 31: Final calibration curve showing experimental data points and linear fit.

accounts for measurement imperfections and small discrepancies due to assumptions in the model (such as perfect clamping and uniform material properties).

With this calibration equation, any future theoretical prediction of the natural frequency can be corrected into its experimental equivalent using:

$$f_{\text{calibrated}} = 1.0140 f_{\text{formula}} - 0.3224.$$

This provides a simple and reliable means of mapping theoretical results to experimental outcomes, ensuring that the coil-magnet measurement system is accurately calibrated across the full frequency

range tested.

## 7 Appendix

### 7.1 Arduino Code

This Arduino code samples an analog signal from pin A0 at a fixed rate using a hardware timer interrupt. The sampling frequency is set to 100 Hz, and data is collected for a total of 4 seconds, resulting in 400 samples stored in the array `SAMPLES`. The sampling is performed inside an interrupt service routine triggered by `Timer1`, which executes at regular intervals determined by the sampling frequency. Each interrupt reads the analog input and stores the value until the specified number of samples has been reached, at which point the timer interrupt is disabled and a flag variable (`FINISHED`) is set. In the main loop, when sampling is complete, all recorded samples are printed to the serial monitor at a baud rate of 57,600, allowing the data to be captured and analyzed later (e.g., for FFT processing).

```
#include <TimerOne.h>    // Include TimerOne library for using hardware
                          timer 1
#include <MsTimer2.h>    // Include MsTimer2 library (not used in this code, but
                          included)

// ***** Constants *****
#define ADC_CHANNEL A0    // Define the analog input channel (A0) for signal
                          sampling

// Sampling configuration
const int SAMPLING_FREQ = 100;           // Sampling frequency in Hz (100
                                          samples per second)
const float TOTAL_SAMPLE_TIME = 4;       // Total sampling duration in seconds
const int NUMBER_OF_SAMPLES = TOTAL_SAMPLE_TIME * SAMPLING_FREQ;
// Total number of samples = sampling frequency    total time (100    4 = 400
samples)

int SAMPLES[NUMBER_OF_SAMPLES]; // Array to store sampled values
long SAMPLING_COUNTER;           // Counter to keep track of how many samples
are taken
bool FINISHED = false;          // Flag to indicate when sampling is complete

void setup () {
    // Initialize the SAMPLES array with -1 (for debugging or to show unused
    entries)
    for (int i = 0; i < NUMBER_OF_SAMPLES; i++) {
        SAMPLES[i] = -1;
    }

    Serial.begin(57600); // Start serial communication at 57,600 baud

    // Configure Timer1 to trigger an interrupt at the sampling frequency
    Timer1.initialize(1e6 / SAMPLING_FREQ); // Timer interval = 1,000,000 s /
    100 Hz = 10,000 s
    Timer1.attachInterrupt(SAMPLING);        // Attach the interrupt service
    routine (ISR) "SAMPLING"
}

void loop() {
    // Main loop runs repeatedly, but actual sampling is done in the ISR
    if (FINISHED) { // When sampling is finished (flag set in ISR)
        for (int i = 0; i < NUMBER_OF_SAMPLES; i++) {
            Serial.println(SAMPLES[i]); // Print each sample value to the serial
            monitor
        }
        FINISHED = false; // Reset flag so samples can be collected again if
        needed
    }
}
```

```

void SAMPLING () {
  // Interrupt Service Routine (ISR) called by Timer1 at fixed intervals
  if (SAMPLING_COUNTER == NUMBER_OF_SAMPLES) {
    // If all required samples are collected:
    Timer1.detachInterrupt(); // Stop the timer interrupt
    FINISHED = true;         // Signal that sampling is complete
  } else {
    // Otherwise, take a new sample
    SAMPLES[SAMPLING_COUNTER] = analogRead(ADC_CHANNEL); // Read analog value
    // from pin A0
    SAMPLING_COUNTER++; // Increment sample counter
  }
}

```



## 7.2 MATLAB code for getting data from Arduino

The MATLAB code acquires sampled data from the Arduino through the serial port at a baud rate of 57,600 and a sampling frequency of 100 Hz for a total duration of 4 seconds, corresponding to 400 data points. The raw data, received as integers from the Arduino's ADC, are converted to voltages using the relation  $V = \frac{ADC}{1023} \times 5$ , assuming a 10-bit ADC with a 5 V reference. The resulting voltage signal is plotted against time to visualize the oscillatory motion of the magnet at a free length of 7 cm for the ruler. To analyze the frequency content, the mean value is removed (centered at 2.5 V), and the Fast Fourier Transform (FFT) is computed. The magnitude spectrum is then normalized and plotted, providing a clear peak at the dominant frequency of oscillation. This allows direct comparison between the measured natural frequency and the theoretical predictions for the ruler setup.

```
clc, clear % Clear the command window and workspace variables
Time = 4; % Total acquisition time in seconds
Fs = 100; % Sampling frequency (Hz)
N = Time*Fs; % Total number of samples = 4 sec * 100 Hz = 400
a = strings(N,1); % Preallocate an array of strings to store serial data

s = serialport("COM4",57600); % Open serial port COM4 at baud rate 57600
configureTerminator(s,"CR/LF"); % Configure line terminator (Carriage Return + Line Feed)

% Read N samples from the serial port line by line
for i = 1:N
    a(i,:) = readline(s); % Read one line from Arduino serial and store as string
end

b = double(a); % Convert string array to numeric (ADC values)
Calib_Metronome_6Hz = b; % Save data in variable for later use
clear s % Close and clear the serial port object

close all % Close any open figures
syms t s % Define symbolic variables (not used later, redundant)

% Convert ADC values to voltages (10-bit ADC, 0{1023 mapped to 0{5 V)
b1 = b/1023*5; % Normalize ADC counts to actual voltage
tt = 1/Fs : 1/Fs : Time; % Time vector for plotting (from 0.01 to 4 sec in steps of 0.01)

% Plot voltage vs. time
plot(tt, b1)
title("Voltage Oscillation VS. Time @ 7 cm (ruler)", "FontName", "Times New Roman");
xlabel("Time (s)", "FontName", "Times New Roman");
ylabel("Voltage (V)", "FontName", "Times New Roman");

% Perform FFT on signal (subtract 2.5 V offset to center around zero)
Y = fft(b1 - 2.5);
Y(1) = Y(1)/2; % Correct DC component scaling
P2 = abs(Y/(N/2)); % Compute two-sided spectrum magnitude
P1 = P2(1:N/2+1); % Convert to single-sided spectrum
P1(2:end-1) = 2*P1(2:end-1); % Double amplitudes (energy conservation)

% Frequency axis for plotting (0 to Nyquist frequency)
f = Fs*(0:(N/2))/N;

% Plot FFT result (magnitude spectrum)
stem(f, P1)
title("Fast Fourier Transform @ 7 cm Hz (ruler)", "FontName", "Times New Roman");
xlabel("Frequency (Hz)", "FontName", "Times New Roman");
```

```

ylabel("Attenuation", "FontName", "Times New Roman");
clc, clear % Clear the command window and workspace variables
Time = 4; % Total acquisition time in seconds
Fs = 100; % Sampling frequency (Hz)
N = Time*Fs; % Total number of samples = 4 sec * 100 Hz = 400
a = strings(N,1); % Preallocate an array of strings to store serial data

s = serialport("COM4",57600); % Open serial port COM4 at baud rate 57600
configureTerminator(s,"CR/LF"); % Configure line terminator (Carriage Return + Line Feed)

% Read N samples from the serial port line by line
for i = 1:N
    a(i,:) = readline(s); % Read one line from Arduino serial and store as string
end

b = double(a); % Convert string array to numeric (ADC values)
Calib_Metronome_6Hz = b; % Save data in variable for later use
clear s % Close and clear the serial port object

close all % Close any open figures
syms t s % Define symbolic variables (not used later, redundant)

% Convert ADC values to voltages (10-bit ADC, 0{1023 mapped to 0{5 V)
b1 = b/1023*5; % Normalize ADC counts to actual voltage
tt = 1/Fs : 1/Fs : Time; % Time vector for plotting (from 0.01 to 4 sec in steps of 0.01)

% Plot voltage vs. time
plot(tt, b1)
title("Voltage Oscillation VS. Time @ 7 cm (ruler)", "FontName", "Times New Roman");
xlabel("Time (s)", "FontName", "Times New Roman");
ylabel("Voltage (V)", "FontName", "Times New Roman");

% Perform FFT on signal (subtract 2.5 V offset to center around zero)
Y = fft(b1 - 2.5);
Y(1) = Y(1)/2; % Correct DC component scaling
P2 = abs(Y/(N/2)); % Compute two-sided spectrum magnitude
P1 = P2(1:N/2+1); % Convert to single-sided spectrum
P1(2:end-1) = 2*P1(2:end-1); % Double amplitudes (energy conservation)

% Frequency axis for plotting (0 to Nyquist frequency)
f = Fs*(0:(N/2))/N;

% Plot FFT result (magnitude spectrum)
stem(f, P1)
title("Fast Fourier Transform @ 7 cm Hz (ruler)", "FontName", "Times New Roman");
xlabel("Frequency (Hz)", "FontName", "Times New Roman");
ylabel("Attenuation", "FontName", "Times New Roman");

```

### 7.3 MATLAB code for calculating ruler's natural frequency

This MATLAB script computes the natural frequency of a cantilevered metal ruler with two cylindrical magnets attached at its free end. Using the material properties of the ruler (Young's modulus, density, dimensions) and the magnet properties (density, diameter, and height), the program calculates the beam stiffness, effective beam mass, magnet mass, and rotary inertia. These are combined into the total effective mass, from which the natural frequency is determined using  $f = \frac{1}{2\pi} \sqrt{k_{\text{tip}}/m_{\text{eff}}}$ . The final frequency value is then printed as the output.

```
clear,clc,close all
% ---- Beam (ruler) ----
E = 193e9;          % Young's modulus [Pa]
b = 26e-3;          % width of ruler [m]
t = 0.5e-3;         % thickness of ruler [m]
L = 0.11;           % overhang length [m]
rho = 7850;         % density [kg/m^3]

% ---- Magnets (NdFeB) ----
rho_mag = 7500;     % kg/m^3
d = 0.015;          % m, diameter
h = 0.020;          % m, length of ONE magnet

% ---- Derived beam props ----
A = b*t;            I = b*t^3/12;
k_tip = 3*E*I / L^3;
m_beam_eff = 0.236 * rho * A * L;
kappa = 1.377;       % phi'(L)/phi(L) for cantilever mode 1

% ---- One magnet mass & inertia (about its own centroid) ----
r = d/2;
m1 = rho_mag * (pi*(d^2)/4) * h;
J1_cm = (1/12)*m1*(3*r^2 + h^2);

Mt = 2*m1;
h_tot = 2*h;
J = (1/12)*Mt*(3*r^2 + h_tot^2); % centroid on beam axis

% ---- Effective inertia & frequency ----
m_eff = Mt + m_beam_eff + (J*(kappa^2)/L^2);
f = (1/(2*pi))*sqrt(k_tip / m_eff);
fprintf('f (with 2 magnets) = %.3f Hz\n', f);
```

## 7.4 MATLAB code for plotting the calibration curve

This MATLAB script plots the experimental frequencies against the theoretical values for the ruler, overlays the fitted calibration line, and displays the calibration curve relating theory to experiment.

```
clear,clc,close all
ruler_cm = [6, 7, 10, 11, 13, 14, 16, 19];
f_formula = [17.719, 14.164, 8.355, 7.243, 5.631, 5.033, 4.109, 3.160];
f_measured = [18, 13.75, 8, 6.75, 5.5, 4.5, 4, 3.25];
f_measured - f_formula
plot(f_formula, f_measured, "o")
hold on
plot(x,y)
title("Calibration Curve")
xlabel("Theoretical (Hz)")
ylabel("Experimental")
legend("Test Data", "Calibration", Location="northwest")
hold off
```